



Published in final edited form as:

*Sci Signal*. ; 11(543): . doi:10.1126/scisignal.aaq1077.

## Identification of Toll-like receptor signaling inhibitors based on selective activation of hierarchically acting signaling proteins

Sirish K. Ippagunta<sup>1,5</sup>, Julie A. Pollock<sup>2,†,‡</sup>, Naina Sharma<sup>2,‡</sup>, Wenwei Lin<sup>3</sup>, Taosheng Chen<sup>3</sup>, Kazuki Tawaratsumida<sup>1</sup>, Anthony A. High<sup>4</sup>, Jaeki Min<sup>3</sup>, Yizhe Chen<sup>3</sup>, R. Kiplin Guy<sup>3</sup>, Vanessa Redecke<sup>1</sup>, John A. Katzenellenbogen<sup>2,\*</sup>, Hans Häcker<sup>1,\*</sup>

<sup>1</sup>Department of Infectious Diseases, St. Jude Children's Research Hospital, 262 Danny Thomas Place, Memphis, TN 38105, USA

<sup>2</sup>Department of Chemistry, University of Illinois at Urbana-Champaign, Urbana, Illinois 61801, USA

<sup>3</sup>Department of Chemical Biology and Therapeutics, St. Jude Children's Research Hospital, Memphis, TN 38105, USA

<sup>4</sup>St. Jude Proteomics Facility, St. Jude Children's Research Hospital, Memphis, TN 38105, USA

### Abstract

Toll-like receptors (TLRs) recognize various pathogen- and host tissue-derived molecules and initiate inflammatory immune responses. Exaggerated or prolonged TLR activation, however, can promote etiologically diverse diseases, such as bacterial sepsis, metabolic and autoimmune diseases, or stroke. Despite the apparent medical need, no small molecule drugs against TLR-pathways are clinically available. This may be because of the complex signaling mechanisms of TLRs, which are governed by a series of protein interactions initiated by Toll-interleukine-1 receptor (TIR)-domains found in TLRs and the cytoplasmic adapter proteins TIRAP and MyD88. Activation/oligomerization of TLRs and consecutive oligomerization of MyD88 and/or TIRAP leads to the recruitment of IRAK family members and the ubiquitin ligase TRAF6. Here, we developed a phenotypic drug screening system based on inducible dimerization of TIRAP, MyD88

\*Corresponding author. hans.haecker@stjude.org (H.H.) or jkatzene@illinois.edu (J.K.).

†Present address. Department of Chemistry, University of Richmond, Richmond, VA 23173, United States

‡Present address: Department of Biotechnology, All India Institute of Medical Sciences, Ansari Nagar, New Delhi, Delhi 110029, India

‡Contributed equally to this project.

**Author contributions:** H.H. conceived and coordinated the project. H.H., J.A.K. and J.A.P. developed the project and wrote the manuscript. S.K.I., J.A.P., N.S., K.T., Y.C. and H.H. performed experiments, and S.K.I., J.A.P., N.S., W.L., T.C., A.A.H., Y.C., J.M., K.G., V.R., J.A.K. and H.H. analyzed and discussed the data. W.L. and T.C. performed HTS. A.A.H. performed MS.

#### SUPPLEMENTARY MATERIALS

Fig. S1. DMSO tolerance of reporter cell lines during stimulation.

Fig. S2. Z'-values of the HEK293T cell-based screening system.

Table S1. Complementary data for Table 1.

Table S2. Complementary data for Table 2.

Supplementary Methods.

**Competing interests:** The authors declare that they have no competing interests.

Data and materials availability: Expression vectors will be provided to researchers who make reasonable requests upon completion of an MTA with the St. Jude Children's Research Hospital. If material is remaining, small quantities of the compounds that were tested as TLR signaling inhibitors will be provided to researchers who make reasonable, research-related requests after completion of an MTA with the University of Illinois at Urbana-Champaign.

and TRAF6, that ranked hits according to the position of action in the hierarchy of the TLR signaling cascade. From a bioactive compound library, we identified methyl-piperidino-pyrazole (MPP) as a TLR-specific inhibitor. Structure-activity relationship analysis, quantitative proteomics, protein interaction assays, and cellular thermal shift assays strongly suggest that MPP targets the TIR domain of MyD88. Chemical evolution of the original MPP-scaffold generated compounds with selectivity for distinct TLRs that interfered with specific TIR interactions. Administration of a MPP-analog to mice protected against LPS-mediated TNF $\alpha$  release. These results validate this phenotypic screening approach and implicate the MPP scaffold as starting point for anti-inflammatory drug development.

## INTRODUCTION

Toll-like receptors (TLRs) are a critical part of the innate pathogen recognition system(1). Comprised of a family of 10 functional receptors in humans, TLRs recognize different pathogen- and host-derived molecules to initiate cellular and inflammatory immune responses(2) (3). They are primarily expressed on innate immune cells and activate a large number of cytotoxic and inflammatory mediators, such as nitric oxide, tumor necrosis factor  $\alpha$  (TNF $\alpha$ ), and interleukin-1 (IL-1). Exaggerated or prolonged TLR-mediated inflammation can lead to pathology in etiologically different diseases, including bacterial sepsis, ischemia reperfusion injury during stroke, systemic lupus erythematosus (SLE), and obesity-related metabolic inflammation(5) (6) (7) (8) (9). TLRs signal through TLR-IL-1R (TIR)-domain containing proteins, which are shared with members of the IL-1 family, including the IL-1R and IL-18R (10) (11) (12). Members of the IL-1 family also stimulate other inflammatory receptors, such as Nod-like receptors (NLR)(13). Therefore, development of small molecule inhibitors of TLR/IL-1R signaling pathways may have broad therapeutic application beyond TLR-mediated inflammation to other diseases, such as NLR-mediated gout(14) (15) (16). Still, despite the pressing need, TLR-inhibitors are not currently clinically available, at least in part due to the complexities of TLR signal transduction (for reviews see (8) (17)). Here, we describe a screening platform for the identification of small molecule inhibitors of TLR-specific signal transduction pathways.

TLR signaling depends on the homotypic protein interactions between the TLR TIR-domain and the TIR-containing intracellular adaptor protein MyD88 (also Myeloid differentiation primary response 88) (Fig. 1A) (11) (18) (19). In most cases, MyD88 binds directly to the intracellular TLR moiety, while in case of TLR2 and TLR4 the TIR-containing protein TIRAP/MAL (Toll/interleukin-1 receptor domain-containing adapter protein/MyD88 adapter-like protein) appears to act as molecular bridge between TLR and MyD88 (Fig. 1A) (20) (21) (22). An exception to this rule is the double stranded RNA-receptor TLR3, whose signaling does not depend on MyD88, but is mediated by two other TIR-containing proteins, TRAM and TRIF(23) (24) (25) (26) (27). Although this 'TRIF-pathway' is also used by TLR4 (23), MyD88 is a critical mediator of TLR4-dependent LPS-induced sepsis(28). Oligomerization of MyD88 results in sequential recruitment of IRAK (Interleukin-1 receptor-associated kinase) family members through death domain interactions(11) (29). IRAK family members then bind and oligomerize TRAF6 (TNF receptor-associated factor 6), which is necessary to activate NF- $\kappa$ B and mitogen-activated protein kinase (MAPK)

downstream signaling pathways (Fig. 1A)(30) (31) (32). Whereas the function of TLR signaling proteins acting upstream of TRAF6 are largely restricted to TLR/IL-1R members, activation of TRAF6 and its downstream targets are used by various receptors and signaling pathways, including members of the TNFR family(33). Consequently, mice deficient in MyD88 do not show overt adverse symptoms unless challenged with infectious agents(12). These mice are also protected from septic shock(28). Similarly, MyD88-deficient humans are more susceptible to bacterial infections during childhood. Yet these patients are largely unaffected as adults, suggesting compensatory mechanisms mediated by other parts of the immune system(34). Together, these data suggest targeting TLR signaling upstream of TRAF6 may be most suitable for development of TLR/IL-1R inhibitors, because even complete inhibition of signal transduction is unlikely to result in unmanageable adverse events.

TLR-mediated cell activation can be mimicked by chemically-induced dimerization of the TLR signaling proteins MyD88 and TRAF6(30) (35). Here, TIRAP was fused to the protein Gyrase B (GyrB), which inducibly dimerizes after exposure to the bivalent antibiotic coumermycin (CM)(36). Expression of TIRAP-, MyD88-, or TRAF6-fusion proteins allowed for selective activation of specific TLR signaling intermediates that recapitulate the hierarchy of signal transduction observed during physiological receptor activation(30). When stably expressed in HEK293T-cells expressing an NF- $\kappa$ B luciferase reporter, this step-wise system of three inducible TLR-signaling proteins allowed us to identify small molecule drugs that interfered with activation of distinct signaling intermediates (Fig. 1A). Using a bioactive compound library, we identified one compound with TLR-specific inhibitory activity, which we further characterized in more detail with respect to mechanism of action, in vivo activity, and developmental opportunities through structure-activity investigations.

## RESULTS

### A high throughput screen identifies TLR-inhibitory compounds

Because genetic and biochemical evidence suggests that TIRAP acts upstream of MyD88 to mediate TLR signaling (20) (37) (21), we fused GyrB to the TIR-domain containing protein TIRAP. When expressed in HEK293T cells, GyrB-TIRAP fusion proteins showed robust CM-inducible signaling activity, similar to fusion proteins of GyrB and MyD88/ TRAF6 (Fig. 1B). To confirm the hierarchical organization of TIRAP acting upstream of MyD88, we deleted MyD88 in GyrB-TIRAP cells by sgRNA-/ CAS9-mediated deletion, which resulted in complete loss of TIRAP-mediated NF- $\kappa$ B activation (Fig. 1C and D) and response to IL-1 $\beta$ , but not TNF $\alpha$  (Fig. 1D). Therefore, GyrB-TIRAP can be used to activate the TLR-pathway upstream of MyD88, recapitulating TLR2- and TLR4-mediated signal transduction.

Three inducible cell lines (TIRAP-GyrB, MyD88-GyrB, TRAF6-GyrB) were optimized for large-scale step-wise 384-well format high throughput screening (HTS). As a primary screen, TIRAP-GyrB cells were used to identify compounds with NF- $\kappa$ B-specific inhibitory activity, and to exclude compounds with non-specific activity (toxicity) (Fig. 2A). We screened a total of 4364 unique compounds from our bioactive compound library, which was acquired from various sources and included 913 FDA (US Food and Drug Administration)-

approved drugs or clinical candidates. Because I $\kappa$ B $\alpha$ -kinase (IKK) is required for NF- $\kappa$ B activation downstream of TRAF6(38) (39), as pathway-specific reference compound we used PS1145, a selective inhibitor of IKK. As non-specific reference compound we used staurosporine, a kinase inhibitor with largely non-selective toxicity(40). DMSO testing demonstrated tolerance of the cell lines up to a concentration of 0.63% DMSO (fig. S1). Assay validation included analysis of within-plate and between-plate variation, which consistently gave Z'-factors of > 0.5, demonstrating the robustness of this phenotypic screening platform (fig. S2). The primary screen criteria identified 213 hits, which were further screened by generating full dose-response curves on all three cell lines (Fig 2A). Compound selectivity was determined by preferential inhibition of signaling initiated by an individual adaptor protein. Compounds that inhibited TRAF6 were eliminated as TLR-'non-specific'. Compounds with selective activity against TIRAP, but not MyD88 and TRAF6 suggest selectivity for the TLR2-/ TLR4-pathway, while activity against TIRAP and MyD88 suggest general or 'Pan'-activity against all TLRs (Fig. 2A). Only 8 compounds exhibited preferential activity against TIRAP or TIRAP/MyD88 over TRAF6 (ratio IC<sub>50</sub> > 5-fold). Tertiary screens were performed with re-synthesized compounds using physiological TLR ligand-mediated stimulation of the RAW264.7 macrophage cell line or primary macrophages (41). Of these, seven of the eight compounds identified were excluded due to lack of activity on RAW264.7 cells or additional activity against cell activation by TNF $\alpha$  or Curdlan, a beta-1,3-glucan that activates cells TLR-independently through Dectin-1 (42).

The remaining compound, methyl-piperidino-pyrazole (MPP), exhibited promising properties. This basic side-chain-containing pyrazole (BSC-pyrazole) is an estrogen receptor alpha (ER $\alpha$ )-selective inhibitor (43). Computational analysis showed that MPP was unique in our bioactive library. MPP inhibited TIRAP- and MyD88-mediated NF- $\kappa$ B activity comparably at low  $\mu$ M concentrations, suggesting it possessed general ('Pan')-TLR-inhibitory activity (Fig. 2B). Consistent with this interpretation, MPP interfered with TNF $\alpha$  release from primary macrophages that were stimulated with CpG-DNA (TLR9), Resiquimod (R848; TLR7), Pam3Cys (TLR2) or LPS (TLR4)(Fig. 2C). In contrast, MPP did not reduce TNF $\alpha$  release induced by Curdlan(42). Thus, MPP interfered selectively with TLR-induced cell activation.

### **MPP inhibits TLR signaling by preventing dimerization of the MyD88 TIR domain**

TLR signaling diversifies downstream of TRAF6 towards multiple well-defined pathways, including the NF- $\kappa$ B and mitogen-activated protein kinase (MAPK) pathways (Fig. 1A)(30) (32). When we investigated the effect of MPP on TLR-induced signaling activation in RAW264.7 cells after CpG-DNA activation, we found that MPP blocked degradation of I $\kappa$ B $\alpha$ , reflecting NF- $\kappa$ B activation, as well as phosphorylation of multiple MAPK pathways almost completely (Fig. 2D). Because we observed no preferential activity towards a specific pathway, these data suggest that MPP acts upstream of TRAF6. MPP also blocked NF- $\kappa$ B- and MAPK-pathway activation downstream of the TLR7 ligand R848, albeit not completely (Fig. 2D). As observed earlier, Curdlan-induced cell activation remained largely unaffected (Fig. 2C and D). Similarly, MPP inhibited TLR9-induced TNF $\alpha$  release and activation of signaling pathways comparably in both wildtype and ER $\alpha$ -deficient bone marrow-derived macrophages (BMM), strongly suggesting the effect of MPP on TLR- and ER $\alpha$  inhibition

are independent events (Fig. 2E and F). Together, the data suggest that MPP blocks the MyD88-pathway upstream of TRAF6, independent of ER $\alpha$  inhibition.

To understand how MPP inhibits TLR signaling, we investigated the assembly of the MyD88 signaling complex after CpG-DNA stimulation. Using stable isotope labeling with amino acids in cell culture (SILAC) and quantitative mass spectrometry (MS) we identified proteins interacting with MyD88 from unstimulated and CpG-DNA-stimulated cells treated with and without MPP. Whereas the bait protein MyD88 was detected at similar amount in all conditions, reflected by protein ratios close to 1 (Fig. 3A), CpG stimulation led to increased interaction between known components of the TLR/MyD88 signaling complex. For example, IRAK4 was identified with 17 unique peptides at 8.4-fold higher amount in CpG-DNA-stimulated samples as compared to unstimulated control samples (Fig. 3A). Strikingly, MPP treatment almost completely blocked recruitment of all activation-dependent MyD88-interacting proteins, including IRAK4, which directly interacts with MyD88(44) (45). We confirmed this finding in small-scale co-immunoprecipitation (co-IP) experiments with antibodies against IRAK4 and TRAF6 (Fig. 3B). These data suggest that MPP blocked a very early event in MyD88 activation.

The currently favored model of MyD88 activation involves TLR-induced, TIR-domain-mediated dimerization of MyD88 as the first step of signal induction, followed by a spiral assembly of further MyD88 molecules(29). When we investigated the effect of MPP on MyD88 homodimerization after TLR stimulation by co-immunoprecipitation, we found that MPP inhibited recruitment of endogenous MyD88 and IRAK4 to GyrB-MyD88 (Fig. 3C). Furthermore, co-IP experiments in HEK293T cells co-expressing the TIR-domain or the DD-domain with full-length MyD88 indicated that MPP strongly reduced the interaction of the TIR-domain, but not the DD-domain, with full length MyD88 (Fig. 3D). Together, these data suggest that MPP inhibited homotypic MyD88 dimerization, thereby preventing assembly of a higher order MyD88 complex, which is required for consecutive recruitment and activation of IRAK4.

To substantiate MyD88 target engagement by MPP, we performed cellular thermal shift assays (CETSA). In these experiments we treated HEK293T cells with an analog of MPP, TSI-13-57, which exhibited similar activity in the low micromolar range, but reduced toxicity in comparison to MPP (Table 2). Cells were heated briefly before lysates were collected and probed by western blot for endogenous MyD88 and actin. TSI-13-57 treatment stabilized and protected MyD88 from temperature-sensitive loss, however, actin was not affected (Fig. 3F and G). Moreover, we found that the concentrations of TSI-13-57 required for MyD88 stabilization and inhibition of TLR-mediated TNF $\alpha$  release corresponded well to each other, with EC<sub>50</sub> values in the low micromolar range (Fig. 3H and I). Together, our results indicate that MPP and its analog TSI-13-57 likely bind directly the TIR-domain of MyD88 to prevent TLR-mediated cell activation.

### **Optimizing the chemical structure of MPP identifies determinants of potency and selectivity**

To understand the chemical requirements for MPP-mediated TLR inhibition, we generated various analogs of MPP (Table 1 and 2, and Table S1 and S2) and assessed their activity by

evaluating TLR9-mediated TNF $\alpha$  production in RAW264.7 cells and ER binding affinity. We found that the appended basic side chain (BSC) at position R5 of MPP's pyrazole core was necessary for the inhibitory activity of MPP, because compound TSI-13-03 that lacked this group did not inhibit CpG oligonucleotide-stimulated TLR9 activity (Table 1, entry 2). By contrast, blocking of the free phenols on N1 and C3 of MPP as methyl ethers decreased ER binding affinity without compromising TLR9 inhibition (Table 1, entry 3), suggesting that TLR9 inhibition and ER $\alpha$  binding may be separable. By substituting side chains of various sizes at position C4 of the pyrazole, we found that smaller groups were preferred (Table 1, entries 1, 4–5) and the presence of a phenol ring was poorly tolerated (Table 1, entry 6). The effect of the substituent on C4 on ER $\alpha$  binding is roughly the opposite as on TLR9 inhibition. From our previous studies on MPP, we know that the location of the BSC can significantly influence the binding affinity for ER(47) (48) (49). As the BSC was moved from C5 to C4 (Table 1, entries 7–8), TLR9 inhibition was retained as was substantial ER $\alpha$  binding and, curiously, affinity for ER $\beta$  increased as compared to MPP. Moving the BSC to C3 (Table 1, entry 9) caused a major decrease in binding affinity to the ERs while retaining TLR9 inhibition. Thus, we identified a chemical modification that limits ER binding without affecting TLR inhibition to limit potential ER-related off-target effects.

When MPP-derived compounds with the BSC on C3 were tested for inhibitory activity against multiple of TLRs and Dectin-1, we found that the location and number of free phenolic groups had a drastic effect on both TLR inhibitory activity and toxicity (Table S2). We noted that compounds with a phenol group at N1 (Table 2, entry 1 and entry 3) only weakly inhibited TLR activity. Movement of the phenol to C5 (Table 2, entry 2) increased potency against all TLRs and decreased toxicity. When both of these phenols were present (Table 2, entry 3), the TLR activity was moderate and toxicity was relatively low. Moving the hydroxyl on the C5 phenyl from the para position to the meta position completely abolished TLR inhibition (Table 2, entry 4), which suggests that there may be some geometrically specific interactions with the phenol or an electronic donating effect of the hydroxyl group into the pyrazole ring that assists with interaction with the TLR target.

As we expanded our scope to include additional functional groups, we observed an interesting result that could lead to selective and specific TLR modulators. For example, compounds that had an electron-withdrawing para-nitro group on N1 only inhibited TLR9 activity (Table 2, entry 5 and Fig. 4A). In contrast, addition of an electron-donating group on the C5 ring restored pan-TLR inhibitory activity (Table 2, entry 6). In addition, removal of the N1 substituent and increased electron-donating capability at C5 resulted in a compound with TLR9- and TLR7-selective activity (Table 2, entry 7 and Fig. 4A). Lastly, replacement of the MPP 1-piperidinyl BSC with a 1-pyrazolyl BSC (Table 2, entry 8 and Fig. 4A) afforded a compound completely selective for TLR7. Thus, our data indicate that slight modifications to the electronic nature of the pyrazole core or alterations to the identity of the BSC can influence the specificity of the compounds.

We speculated that the apparent selectivity in TLR-inhibition might reflect preferential interference with specific TIR-domain interactions. To test this possibility we established a mammalian two-hybrid (M2H) system that allowed analysis of specific protein interactions quantitatively. Like the yeast two-hybrid system, this assay is based on the reconstitution of

the function of a transcriptional activator in transfected HEK293T cells that drives expression of a luciferase reporter. In the presence of either a TLR9-selective (TSI-13-48) or pan-TLR (TSI-13-57) inhibitor, we tested the interaction of MyD88 with MyD88, TLR9 with MyD88, and TIRAP with MyD88 (Fig. 4B). Consistent with earlier data (Fig. 3E–H), we found that TSI-13-57 inhibited homodimerization of the TIR-domain of MyD88, but showed little inhibitory activity on the interaction between TLR9 and MyD88, and no activity against interaction between TIRAP and MyD88 (Fig. 4B). In marked contrast, TSI-13-48 did not affect homodimerization of MyD88 TIR or interaction between TIRAP and MyD88, but reduced interaction between TLR9 (TIR) and MyD88 (Fig. 4B). Of note, the IC<sub>50</sub> values obtained in this M2H system matched closely those obtained during physiological TLR activation of macrophages, both with respect to inhibition of MyD88-dimerization by TSI-13-57 and inhibition of TLR9 (TIR) - MyD88 interaction by TSI-13-48 (Fig. 4A, B and Table 2). Thus, modifications of the MPP scaffold that generate compounds with selective activity against specific TLRs, block specific TIR-domain interactions.

### An MPP analog protects mice from sepsis in vivo

Release of the gram-negative cell wall component LPS (or endotoxin) is the basis of sepsis, mediated through TLR4 and executed by TNF $\alpha$ -induced liver injury(5) (50).

Characterization of the in vivo pharmacokinetics of TSI-13-57 showed a dose-dependent increase in the maximum serum concentration (C<sub>max</sub>) after intra-peritoneal (i.p.) administration and a plasma half-life of 9.0 hours (Table 3). No significant changes in hematological parameters, clinical chemistry, or gross organ anatomy were observed at the terminal point of the study, corresponding to the lack of apparent toxicity against various cell lines in vitro (Table 4). Mice treated with either 100 mg/kg and 200 mg/kg TSI-13-57 were challenged with LPS. Analysis of the TNF $\alpha$  concentration in the serum 90 min after challenge indicated that low dose treatment reduced systemic inflammatory responses to TLR stimulation, and high dose treatment almost completely blocked LPS-induced TNF $\alpha$  release (Fig. 5A). In vivo inhibitory activity correlated well with plasma concentrations of TSI-13-57 and its known in vitro IC<sub>50</sub> of 6.73  $\mu$ M for LPS-induced TNF $\alpha$  release from macrophages (Fig. 4A and Table 2). These data provide proof of principle that MPP analogs with TLR-inhibitory activity can be used to counteract TLR-induced effector functions in vivo.

## DISCUSSION

The screening approach presented resembles other phenotypic screening methods where a series of events that lead to a complex phenotype are interrogated for perturbation by compound libraries. An important advantage of phenotypic screening is that not only known, but also unknown cellular mechanisms can be explored. In particular, molecular events that are more difficult to recapitulate in vitro, such as dynamic protein interactions, which are less amenable to targeted drug development, can be investigated during their physiological function in the natural context in living cells. The major disadvantage of phenotypic screening approaches is that the identity of the drug target remains unknown, and criteria to prioritize hit series are primarily driven by the chemical nature of the compounds. The labor-intensive identification process may postpone the discovery of the actual drug target, which

may reveal undesirable properties. Thus, the process from hit identification to target validation can be time consuming and difficult.

Our screening approach addresses these problems by two particular features. First, based on artificially activated, hierarchically acting signaling molecules, we narrow the phenotypic window to a (largely) defined process of signaling events that are known to be restricted to TLR-signaling pathways. Although this procedure adds additional effort to the screening procedure itself, it simplifies drastically the following steps of drug target identification. We took advantage of GyrB-mediated induced proximity (dimerization), which allowed us to activate distinct intermediates in the TLR signaling cascade. Given that induced proximity is a common principle in signal transduction, it is likely that similar screening paradigms can be developed for other signaling pathways. Second, we developed a method to assess quantitatively the entire signaling process in question using SILAC-based quantitative MS, which captures the assembly of all essential components of the TLR-specific pathway. The first aspect allowed us to reduce the number of 213 hits to only 8 compounds, whose analysis in more detailed, yet still relatively simple assays, could be managed with reasonable effort. The second aspect, the recapitulation of the phenotypic signaling window by quantitative MS, allowed us to focus on MyD88 dimerization as the most likely affected mechanism, an interpretation that was supported by additional evidence based on Co-IPs, two-hybrid assays, and CETSA. Our attempts to further characterize drug target interaction, such as thermal shift assays based on recombinant protein or structural analyses based on X-ray co-crystallography, were impeded by unfavorable properties of the recombinant MyD88 TIR domain (MyD88-TIR), most likely due to protein aggregation. MyD88-TIR had been crystallized before using co-incubation with the *Escherichia coli* protein TcpC to prevent aggregation(51). Possibly, a similar strategy could be used to support structural investigation of the interaction between compound and MyD88, which may guide future compound optimization. While in vitro and in vivo PK analyses did not reveal apparent liabilities of the compounds investigated, improved potency will be an important goal for optimization and will facilitate further in vivo testing, in particular in long-term studies. Together, our work validates a novel phenotypic screening approach and identifies one chemotype with highly selective TLR-inhibitory activity.

The relative scarcity of TLR signaling inhibitors developed based on targeted approaches highlights the strategic opportunity of this screening approach. One interesting compound, the peptidomimetic ST2825, was developed based on the BB-loop peptide of MyD88-TIR, which contributes to MyD88 dimerization(52) (53). Consistent with the expected mechanism of action, ST2825 blocked MyD88 dimerization, IRAK recruitment and signal transduction. Potency of ST2825 was, however, relatively modest with an  $IC_{50} > 10 \mu M$  for IL-1 $\beta$ -induced NF- $\kappa B$  activity(53). Another compound, C29, was selected as TLR2-specific compound based on computer-aided drug design, and was shown to reduce TLR2-mediated cell activation (54). Potency, however, was low ( $IC_{50} \approx 20 \mu M$ ), and toxicity and therapeutic window were not assessed. Thus, alternate strategies to identify TLR signaling inhibitors are warranted.

Another, emerging class of compounds that interfere with TLR-mediated inflammatory responses are IRAK4 kinase inhibitors. While these inhibitors take advantage of a defined



structure for targeted drug development, the specific pathway and cell functions controlled by IRAK4 kinase activity are less certain. In contrast to the scaffolding function of IRAK4, which is essential for canonical signaling pathways such as NF- $\kappa$ B, the kinase function of IRAK4 appears to play a minor role in canonical TLR-pathways, but rather controls a subset of TLR-induced genes in a monocyte-specific way, possibly through mRNA stabilization (55) (56) (44) (57) (58). Still, inhibition of IRAK4 kinase activity in monocytes results in strongly reduced cytokine production (55) (57) and an increasing number of chemically diverse, selective kinase inhibitors have been developed, several of which demonstrated in vivo efficacy in proof of principle models (59) (60) (61) (62) (63) (64) (65) (66) (67) (68). While most IRAK4 inhibitors showed in vivo PK properties requiring further improvement, a very recently published compound, Pf-06650833, showed remarkable in vivo potency (2.4 nM IC<sub>50</sub> on R848-induced PBMC) and selectivity, and has been moved forward to clinical studies(69). Taken together, IRAK4 inhibitors represent an interesting class of TLR inhibitors with a most likely more selective interference with TLR biology. Thus, the therapeutic impact of IRAK4-inhibitors is expected to be different from TSI identified in this study or genetic loss of function models. Comparing the effects of TSI and IRAK4 kinase inhibitors will be an important future goal, possibly establishing specific therapeutic indications for the two classes of compounds.

A particularly interesting observation of the MPP-derived compounds described in this study was their developmental potential towards inhibition of specific TLR pathways. While the original compound, MPP, displayed Pan-TLR inhibitory activity and had high ER $\alpha$  binding affinity, through our structure-activity relationship studies we were quickly able to make modifications to the substituents on the pyrazole core that eliminated binding to both ER $\alpha$  and ER $\beta$  while retaining and improving potency as TSIs. In addition to compounds that were inhibitory for TLR2/4/7/9 (Pan-TLR antagonists), a number of compounds emerged having highly selective activity against TLR7-, TLR9- and TLR7/TLR9-induced cell activation. Compounds with selectivity for specific TLRs (or a combination thereof) are particularly interesting with respect to diseases that are mediated by defined TLRs, for example SLE, which appears primarily promoted by the nucleic acid-recognizing TLRs, TLR7 and TLR9(70). TLR2/4-selective compounds were not identified. The pan-TLR and TLR9-selective activity of TSI-13-57 and TSI-13-48 correlated with their interference with MyD88 TIR homodimerization and interaction between TLR9 and MyD88, respectively. These data suggest that selectivity is governed by interference with specific TIR domain interactions. Still, the molecular mechanism controlling selectivity is unclear. We favor a model where all compounds bind to the MyD88-TIR, whose engagement by up-stream TIRs may involve structurally distinct motifs, which may be differentially affected by specific compounds. Alternatively, different compounds could bind to homologous regions of different TIR domains. It is likely that structural data will be required to delineate the precise mechanism of action. In any case, we expect that understanding the molecular basis of compound activity and selectivity will contribute to our understanding of the molecular mechanism of TLR signal transduction and, hopefully, successful future drug development.

## MATERIAL AND METHODS

### Reagents and plasmids

CpG-DNA refers to the phosphothioate backbone containing oligonucleotide 1668 (TCCATGACGTTCCCTGATGCT) (TIB Molbiol). Other agonists used were LPS (*Escherichia coli* 0127:B8) (Sigma-Aldrich), coumermycin A1 (Sigma-Aldrich), R848 (GLSynthesis), tripalmitoyl cysteinyl lipopeptide (Pam3Cys) (EMC Microcollections) and Curdlan (InvivoGen). The following antibodies were used: FLAG (M2 [soluble and bead immobilized]),  $\beta$ ACTIN (Sigma-Aldrich), MyD88, I $\kappa$ B $\alpha$ , P-p38, P-JNK, P-ERK, p38 and Myc-Tag (Cell Signaling Technology), HA (Roche); secondary antibodies conjugated to horseradish peroxidase (GE Healthcare Life Sciences). Chemiluminescent substrate was from Thermo Scientific. ELISA kits were from eBiosciences (TNF- $\alpha$ ). Luciferase assay system was from Promega. Alamar blue assay system and Lipofectamine 2000 was from Invitrogen. Full length human ER $\alpha$  and ER $\beta$  were obtained from PanVera/Invitrogen (Carlsbad, CA); tritiated estradiol was obtained from Perkin-Elmer (Waltham, MA).

Expression plasmids were established by conventional molecular biology techniques and verified by DNA sequencing. Epitope tags used consisted in tandem triple tags (HA, FLAG) or single tag (Myc) which were fused N-terminal to the cDNA of full length MyD88, the MyD88 death domain (aa 2–109) or the MyD88 TIR-domain (aa 157–296). FLAG-tagged TIRAP-Gyrase B was expressed as fusion protein consisting in triple-FLAG-tagged, full-length TIRAP and a C-terminal Gyrase B moiety using a lentiviral vector containing a PGK1-promoter. FLAG-tagged MyD88-GyrB was expressed as fusion protein consisting in triple-FLAG-tagged, full-length MyD88 and a C-terminal Gyrase B moiety using a MSCV-based retroviral vector (MSCV-puro (Clontech)). FLAG-tagged TRAF6-GyrB was expressed as fusion protein consisting in a triple-FLAG-tagged, N-terminal part of TRAF6 (aa 2–351) and a C-terminal Gyrase B moiety using a pcDNA3-based vector with EF1 $\alpha$  promoter.

### Reporter cell lines

To establish NF- $\kappa$ B-responsive luciferase reporter cells lines, HEK293T cells were transduced with a lentiviral vector containing a luciferase reporter gene under control of three NF- $\kappa$ B-binding sites. Single cell clones of transduced cells were established by limiting dilution, and inducible NF- $\kappa$ B activity was confirmed by transfection with various TLR adaptor proteins. Stable reporter cell lines expressing GyrB-fusion proteins were established by viral transduction (MyD88-GyrB, TIRAP-GyrB) or lipofectamine transfection (TRAF6-GyrB), followed by antibiotic selection. Stably growing cells were cloned by limiting dilution, and clones that showed CM-mediated NF- $\kappa$ B activation were selected for further experiments.

### Cell culture and retrovirus generation

HEK293T cells were cultured in DMEM (Life Technologies), supplemented with 10% (v/v) FCS (Hyclone), 50  $\mu$ M 2-mercaptoethanol, antibiotics (penicillin G (100 IU/ml) and streptomycin sulfate (100 IU/ml)) and pyruvate (1 mM)). RAW264.7 cells were cultured in RPMI 1640 (Life Technologies), supplemented with 10% (v/v) FCS (Hyclone), 50  $\mu$ M 2-

mercaptoethanol and antibiotics (penicillin G (100 IU/ml) and streptomycin sulfate (100 IU/ml)), as described(30, 71). Bone marrow (BM)-derived macrophages (BMM) were generated by cultivating unfractionated BM cells (obtained from female C57BL/6 mice or ER $\alpha$ -deficient mice (*Esr1<sup>tm1Ksk</sup>*(72), The Jackson Laboratories) and corresponding wildtype control mice, as indicated in figure legends) for 6 d in DMEM (Invitrogen), supplemented with 10% (v/v) FCS (Hyclone), 50 mM 2-mercaptoethanol, antibiotics (penicillin G (100 IU/ml) and streptomycin sulfate (100 IU/ml); Invitrogen) and 30% L-cell-conditioned medium as described(73).

For testing of compounds, RAW264.7 cells were seeded in complete RPMI 1640 (without phenol red) medium in 96 well plates at cell a density of 50,000 per well at least 12 hours before stimulation. Cells were treated with compounds in dose response settings (50  $\mu$ M to 0.023  $\mu$ M in three-fold dilutions) or DMSO for 30 min followed by stimulation with various physiological TLR agonists at pre-determined, roughly equi-effective concentrations (CpG DNA (1  $\mu$ M), R848 (300 nM), Pam3Cys (100 ng/ml), LPS (10 ng/ml)) or Curdlan (100  $\mu$ g/ml). TNF $\alpha$  concentrations were determined in cell culture supernatants 6 hours post stimulation by ELISA, and cell viability was analyzed by the Alamar blue assay system (Invitrogen).

Replication-deficient lentivirus and murine stem cell virus (MSCV) was generated based on Lipofectamine 2000 (Invitrogen)-based transient transfection of HEK293T cells using a four-plasmid system that was generously provided by Dr. Inder Verma (for lentivirus), or an ecotropic, MSCV-based two-plasmid system. Cas9-mediated deletion of MyD88 was done by lentiviral delivery of MyD88-specific sgRNA (genomic target sequence: GTTCTTGAACGTGCGGACAC) that was expressed by the lentiviral vector LentiCrisprV2 provided through Addgene(74). Transduced cells were selected with puromycin (10  $\mu$ g/ml) and used as polyclonal cell population.

### Bioactive compound library

The St. Jude 'bioactive' compound library used in this study consisted of 4,364 unique compounds (a total of 8,904 compounds including replicates) acquired from commercial sources (Microsource, Prestwick and Sigma-Aldrich) and external academic collaborators, or synthesized in-house by our chemistry group. It includes FDA approved drugs or clinical candidates (913), nuclear hormone receptor ligands (108), the GSK published kinase toolset (358), kinase inhibitors (1,642), nuclear hormone receptor-based pharmacophore library (744), artemisinin-like compounds (535), certain rare chemical scaffolds (1,665) and some other chemicals with reported biological activities (2,939). The purity of purchased and in-house prepared chemicals was >85% and >90%, respectively. All chemicals were solubilized in DMSO at a stock concentration of 10 mM.

### High Throughput Screening

The TIRAP-GyrB, MyD88-GyrB and TRAF6-GyrB cell lines were stored in multiple aliquots as frozen stocks and thawed for HTS in a standardized manner 10 days (5 passages) before HTS. Phenol red-containing standard DMEM medium which replaced by growth medium without Phenol red during HTS assays. The concentration of FCS was not

optimized towards lower concentrations, as all follow-up experiments had been established at 10%. In the primary high throughput screening, TIRAP-GyrB cells (10,000 cells in 25  $\mu$ l assay medium) were seeded in white 384-well solid bottom tissue culture-treated plates (PerkinElmer) with a WellMate dispenser (Thermo Scientific Matrix) and plates were incubated in an automated tissue culture incubator (Liconic Instruments). After 24 hour incubation, DMSO stock solutions of test chemicals (the St. Jude Bioactive collection), along with coumermycin A1 (Sigma), PS-1145 (Sigma), staurosporine (LC Laboratories) or DMSO (Fisher Scientific) were transferred with a Pin Tool (V&P Scientific) equipped with a 10H pin head to give a final test chemical concentration of 12  $\mu$ M, along with 100 nM coumermycin A1 (one replicate per compound). In addition, groups of wells with 100 nM coumermycin A1 alone, and 100 nM coumermycin A1 with 30  $\mu$ M PS-1145 or 40  $\mu$ M staurosporine were included in each plate as well. The final DMSO concentration in each well was 0.24%. 24 hours later, each plate was treated with 5  $\mu$ l/well DPBS (Fisher Scientific) diluted (1-to-12 dilution) AlamarBlue (Invitrogen), incubated at 37  $^{\circ}$ C for 1 hour, cooled down to room temperature for 15 min, followed by fluorescence analysis using an Envision HTS microplate reader (PerkinElmer, Waltham, MA). Next, the luminescence signals were measured using SteadyLite HTS luminescence assay reagent (PerkinElmer) and the Envision plate reader. In the AlamarBlue cell toxicity assay, the 40  $\mu$ M staurosporine with 100 nM coumermycin A1 group and the 100 nM coumermycin A1 alone group were assigned as the positive (100% inhibition) and negative (0% inhibition) controls, respectively. In the luminescence assay, the 30  $\mu$ M PS-1145 with 100 nM coumermycin A1 group and the 100 nM coumermycin A1 alone group were assigned as the corresponding positive (100% inhibition) and negative (0% inhibition) controls. Test compound activity was normalized to those of positive and negative controls in the individual assays. 213 unique chemicals with luminescence inhibitory activity  $\geq$  50% as well as with AlamarBlue cytotoxic inhibitory activity  $\geq$  20% were selected for further dose response confirmation testing.

In the dose confirmation tests, the basic primary screening protocol was followed with minor modifications, including that 10 concentrations from 56  $\mu$ M to 2.8 nM, along with 100 nM coumermycin A1 in triplicates were tested. The activity data for individual chemicals were fit into sigmoidal dose-response curves if applicable to derive  $IC_{50}$  values with GraphPad Prism 7.00 (GraphPad Software).

### Calculation $Z'$ values

The  $Z'$  values were calculated using the equation  $Z' = 1 - \frac{3\sigma^+ + 3\sigma^-}{Mean^+ - Mean^-}$  (79).  $\sigma^+$  is the standard deviation of the negative control group (negative control groups in the luciferase reporter assay and AlamarBlue cytotoxicity assay for each cell line as defined above),  $\sigma^-$  is the standard deviation of the positive control group (positive control groups in the luciferase reporter assay and AlamarBlue cytotoxicity assay for each cell line as defined above);  $Mean^+$  is the mean of the negative control group, and  $Mean^-$  is the mean of the positive control group.

## Affinity purification and quantitative mass spectrometry

For stable isotope labeling by amino acids in cell culture (SILAC), RAW264.7 cells expressing stably a FLAG-tagged form of MyD88-GyrB were cultured in arginine- and lysine-free RPMI (Invitrogen) supplemented with 10% dialyzed FBS (Invitrogen), penicillin-streptomycin, and either L-arginine and L-lysine (light), L-arginine-HCl (13C6; CLM-2265 [R6]) and L-lysine-2HCl (4,4,5,5 D4; DLM-2640 [K4]) (medium) or L-arginine-HCl (13C6, 15N4; CLM-539 [R10]) and L-lysine-2HCl (13C6, 15N2; DLM-291 [K8]) (heavy) (Cambridge Isotope Labs)(75). For complete incorporation of labeled amino acids, cells were passaged three times in SILAC medium over a period of 5 days. The labeled cells were treated with 10  $\mu$ M MPP for 20 min (heavy), followed by stimulation with 1  $\mu$ M CpG-DNA for 60 min (medium and heavy). The medium was replaced by ice-cold PBS and cells were collected by cell scraping and centrifugation. Cell pellets were incubated with lysis buffer (LB; 20 mM Hepes/NaOH (pH 7.5), 1.5 mM MgCl<sub>2</sub>, 150 mM NaCl, 1 mM EDTA, 10% glycerol, 10 mM  $\beta$ -glycerophosphate, 5 mM 4-nitrophenyl-phosphate, 10 mM sodium fluoride, complete protease inhibitors (Roche)) supplemented with 0.5 % NP-40 for 20 min. Samples were cleared by centrifugation and loaded five times over M2 FLAG-bead-containing columns. Unbound proteins were removed by washing column with LB plus 0.1% NP-40, and proteins were eluted at pH 3.5 in water supplemented with 100 mM glycine, 50 mM NaCl, 0.1% NP-40, and Roche complete protease inhibitors. The proteins were concentrated by trichloroacetic acid precipitation and dissolved in SDS PAGE loading buffer (Bio-Rad). The dissolved proteins were combined, followed by separation on a 10 % Bis-Tris gel (Bio-Rad) and staining with SYPRO Ruby protein stain (Invitrogen). The entire lane was cut into individual bands and analyzed by LC-tandem MS (LC-MS/MS) using a nanoAcquity UPLC (Waters) coupled to an Orbitrap ELITE high resolution mass spectrometer (Thermo Fisher).

### Sample preparation and liquid chromatography-coupled electrospray

**ionization (ESI)**—The protein gel bands were reduced with DTT and alkylated with iodoacetamide and then digested overnight with trypsin (Promega). The digest was introduced into the instrument by on-line chromatography using reversed-phase (C18) ultra-high-pressure LC on a nanoACQUITY UPLC (Waters). The column used was a Waters BEHC18 with an inner diameter of 75  $\mu$ m and a bed length of 10 cm. The particle size was 1.7  $\mu$ m. Tryptic peptides were gradient eluted over a gradient (0 to 70% B for 60 min and 70 to 100% B for 10 min, where B was 70% [vol/vol] acetonitrile, 0.2% formic acid) using a flow rate of 250 nl/min into the high resolution Orbitrap ELITE through a noncoated spray needle with voltage applied to the liquid junction.

### Tandem mass spectrometry (MS/MS) using a hybrid ion trap-orbitrap mass spectrometer (LTQ Orbitrap XL)

—Data-dependent scanning was incorporated to select the 20 most abundant ions (one microscan per spectrum; precursor isolation width, 2.0 Da; 35% collision energy; 10-ms ion activation; 15-s dynamic exclusion duration; 5-s repeat duration; and a repeat count of 1 from a full-scan mass spectrum at 60,000 resolution for fragmentation by collision-activated dissociation). Database searches were performed using RAW files in combination with Andromeda search engine that is part of the MaxQuant software (version 1.1.1.32) developed at the Max Planck Institute(76). The SwissProt

2012\_08 ((537,505 sequences; 190,795,142 residues); Taxonomy: *Mus musculus* (16,605 sequences)) database was used for peptide and protein identification. MaxQuant was also used to quantitate peptides and proteins and to provide ratios generated in Excel format. Protein assignments were made on the basis of both MS and MS/MS spectra, whereas peptide quantitation was based solely on MS data. The following residue modifications were allowed in the search: carbamidomethylation on cysteine (fixed modification), oxidation on methionine (variable modification), label:13C(6) on arginine, label:13C(10) on arginine, label:13C(4) on lysine, and label:13C(8) on lysine. The MS1 mass tolerance was set to 15ppm and the MS/MS tolerance was set to 0.5 Da and protein FDR was set to 0.01. The identifications from the automated search were verified by manual inspection of the raw data.

### Immunoprecipitation

Immuno-precipitation (IP) studies were performed in HEK293T cells that were transfected using Lipofectamine (Life Technologies) with epitope-tagged forms of MyD88. MPP or DMSO was added 7 hours after transfection. 20 h after transfection, cells were lysed for 20 min at 4 °C in lysis buffer (20 mM HEPES/NaOH (pH 7.5), 1.5 mM MgCl<sub>2</sub>, 150 mM NaCl, 1 mM EDTA, 0.5% Nonidet P-40 and 10% glycerol) supplemented with complete protease inhibitors (Roche Applied Science). After clearance of lysates by centrifugation (10 min, 20,817 g, 4 °C), lysates were subjected to immunoprecipitation (IP) using FLAG M2 resin (Sigma-Aldrich) for 1 h at 4°C. IP samples and total cell lysates were analyzed by immunoblotting.

### Cellular thermal shift assay (CETSA)

CETSA was performed as described(78). Briefly, HEK293T cells were treated with TSI-13-57 or DMSO as control at 37°C with 5% CO<sub>2</sub> for 60 min in cell culture dishes (TPP). Cells were resuspended in medium and spun down at 240 g for 5 min at room temperature. Medium was carefully removed and cells were resuspended in phosphate buffered saline (PBS). Cells were spun down again at 240 × g for 5 min at room temperature. PBS was carefully removed again and the cell pellet was resuspended in PBS supplemented with protease inhibitors to obtain a cell density of 8 × 10<sup>6</sup> cells/ml. The cell suspension (0.8 million in 100 µl volume) was transferred to multiple tubes in a real-time PCR plate (Applied Biosystems). The PCR plate was loaded to the heating block of a PTC-200 Gradient Thermocycler (MJ Research) at 25°C. Samples were heated to their desired temperatures in parallel by applying a temperature gradient covering a range between 40°C and 64°C. The respective temperatures were maintained for 3 min before the samples were cooled and maintained at 25°C for 3 min. Next, the tubes were immediately shock-frozen in liquid nitrogen. Cells were lysed by two alternating thaw-freeze cycles in a heating block (25°C) and in liquid nitrogen, respectively. The resulting suspensions were centrifuged at 20,000 g for 20 min at 4°C. For the following steps the lysates were kept on ice. Supernatants of each sample were carefully transferred to reaction tubes without touching or disturbing the pellets and were analyzed by sodium dodecyl sulfate polyacrylamide gel electrophoresis (SDS-PAGE) followed by Immuno-blot analysis.

### Chemical Synthesis, Compound Identity and Purity

A full description of synthetic routes and details of methods, compound purity, and spectroscopic characterization are provided in the Supplemental Information. The purity of all compounds tested for biological activity was >95%, established by <sup>1</sup>H NMR spectroscopy at high concentrations.

### Estrogen Receptor Binding Assay

Competitive radiometric binding assays were performed on 96-well microtiter filter plates (Millipore), using full length human estrogen receptor  $\alpha$  and  $\beta$ , with tritiated estradiol as tracer, as previously described(77). After incubation on ice for 18–24 h, ER $\alpha$ -bound tracer was absorbed onto hydroxyapatite (BioRad), washed with buffer, and measured by scintillation counting. RBA values are the average  $\pm$ SD of 2–3 determinations, unless determined to be < 1/1000 of estradiol (RBA values < 0.1), then one experiment was performed.

### Mammalian two-hybrid assay

Plasmids used for M2H assays were based on the Checkmate mammalian two-hybrid system (Promega). The TIR domain of MyD88 (aa 158–296) was cloned into the Gal4-vector (pBIND) and VP16-vector (pACT), full length MyD88 was cloned into pACT, the TIR domain of TLR9 (aa 867–1032) was cloned into pBind, and TIRAP (aa 1–241) was cloned into pBind. HEK293T cells were transiently transfected with bait- and prey plasmids in 96 well format using Lipofectamine (2000), along with a Gal4-driven firefly luciferase reporter plasmid (pGL5-luc, Promega) and Renilla luciferase control vector (Promega). DMSO or compound was added to cells 7 hours post transfection. Cells were harvested 13 hours later, and luciferase activity was determined using the dual luciferase kit (Promega). Firefly luciferase activity values were normalized to Renilla luciferase activity.

### In vitro analysis of absorption, distribution, metabolism, excretion and toxicity (ADMET)

Solubility assays were carried out on a Biomek FX lab automation workstation (Beckman Coulter, Inc., Fullerton, CA) using  $\mu$ SOL Evolution software (pION Inc.). 16.7  $\mu$ M compound stock solutions (in DMSO) were used to make the reference plate. 0.1 mM compound stock was use in storage plate and incubated at RT for 18 h. The suspension was then filtered through a 96-well filter plate (pION Inc.), diluted with 1-propanol to make the sample plate, and the UV spectrum of the reference and sample plate were read. Calculations were carried out with  $\mu$ SOL Evolution software based on the area under the curve (AUC) of the UV spectrum of the sample and reference plates. All compounds were tested in triplicate. For analysis of permeability, a parallel artificial membrane permeability assay (PAMPA) was conducted with the same instrument using PAMPA Evolution 96 Command software (pION Inc.). 50  $\mu$ M compound stock was used to make the reference plate, and the UV spectrum of this plate was read. GIT lipid (pION Inc.) was used as the membrane on the pre-loaded PAMPA Sandwich (pION Inc.). The acceptor and donor chamber of the sandwich was then filled with 200  $\mu$ L of acceptor solution buffer (ASB) (pION Inc.) and test compound. The PAMPA Sandwich was assembled, placed on the Gut-box, and stirred for 30 min. Then the UV spectrum of the donor and the acceptor were read.

The permeability coefficient was calculated based on the AUC of the reference plate, the donor plate, and the acceptor plate. All compounds were tested in triplicate. Cytotoxicity studies were based on BJ (human foreskin fibroblasts), HEK293 (human embryonic kidney cells), HepG2 (human hepatocellular carcinoma cells), and Raji (human lymphoblast cells (Burkitt's lymphoma)) cell lines (American Type Culture Collection (ATCC), Manassas, VA), which were cultured according to recommendations and cell culture media from ATCC. Exponentially growing cells were plated in 384-well white custom assay plates (Corning) and incubated overnight at 37 °C in a humidified 5% CO<sub>2</sub> incubator. DMSO inhibitor stock solutions were added the following day to a top final concentration of 25 µM of 0.25% DMSO and then diluted 1/3 for a total of ten testing concentrations. Cytotoxicity was determined following a 72 hour incubation using Cell Titer Glo Reagent (Promega), according to the manufacturer's recommendation. Luminescence was measured on an Envision plate reader (Perkin Elmer).

Compound stability was assessed using mouse liver microsomes (20 mg/ml microsomes) in potassium phosphate buffer (0.1M, pH 7.4). 10 mM stocks of compound in DMSO were diluted with DMSO and acetonitrile to three different intermediate concentrations. Only one concentration of controls (diphenhydramine HCl, verapamil HCl, and Ketoprofen) was used. Each diluted compound stock (37.83 µL) was added to an aliquot of the liver microsomal solution (3 ml), vortexed, and transferred to five 96-well assay plates. A single assay plate was tested at each time point: 0 hour, 0.5 hours, 1 hour, 2 hours, and 4 hours. For 0-hour time point, pre-cooled (4 °C) internal standard (2 µM warfarin in Methanol) was added to the plate before the reaction starts. For other time points, NADPH solution (Fisher Scientific) was added first. The plates were sealed, and all plates except the 0-hour plate were incubated at 37 °C, shaken at a speed of 60 rpm. At each time point, 437.5 µL of pre-cooled internal standard was added to quench the reaction. The final compound concentrations were: 20 µM, 4 µM, and 0.8 µM. The concentration of controls was 4 µM. The quenched plate was then centrifuged at 4000 rpm for 15 min at 4 °C. Resulting supernatant was transferred to a 96-well plate and analyzed by UPLC-MS (Waters Inc., Milford, MA). The compounds and internal standard were detected by selected ion recording (SIR). The amount of material was measured as a ratio of peak area to the internal standard and graphed. Using the slope from the most linear portion of this curve, the degradation rate constant is calculated. The rate constant was then used to calculate the compounds half-life in plasma. Intrinsic clearance was calculated as  $CL_{int} = (0.693 / (t_{1/2})) * (1 / \text{microsomal concentration in the reaction solution}) * (45 \text{ mg microsomes/gram liver}) * (\text{gram liver/kg b.w.})$ , where microsomal concentration in the reaction solution is 0.5 mg/ml, and gram liver/kg b.w. of mouse is 52.

### **In vivo pharmacokinetic study**

Female C57BL/6 mice with average weight of 19 grams were purchased from Charles River Laboratories (Wilmington). Food and water were provided ad libitum. 15 mice were divided into three dosage groups: 0, 10 and 20 mg/kg. For each mouse, 0.1 ml of compound suspension in formulation (0.5% CMC, 0.4% Tween 80) was given by intra-peritoneal (i.p.) injection. 0.1 ml blood was collected retro-orbitally from a different mouse within each dosage group at 5 min, 15 min, 30 min, 1 hour, 4 hour, and 24 hour. Animals were



Author Manuscript

euthanized by cardiac puncture at 48 hour post injection. Blood samples were treated with 10  $\mu$ L of EDTA sodium solution to prevent coagulation. Blood was kept on ice and centrifuged for 3 min at 13,000 rpm in a desktop centrifuge to collect plasma. 25  $\mu$ L plasma samples were combined with 75  $\mu$ L internal standard (2  $\mu$ M warfarin) in acetonitrile in a 96 well plate and centrifuged at 4000 rpm for 20 min at 4 °C. The supernatant (40  $\mu$ L) was collected and mixed with 2 part of Milli-Q water (EMD Millipore) and centrifuged again at 3000 rpm for 20 min at 4 °C. Plasma concentration was determined with partially validated LC/MS-MS assay with MRM detection (AB Sciex). The assay limit of quantification (LLOQ) was 1.5 nM in plasma.

Author Manuscript

The processed plasma concentration-time data were analyzed using non-compartmental analysis (NCA) in WinNonlin 6.0 with the Plasma (200–202) model type..

The Area Under the Concentration-Time Curve (AUC) was calculated with the linear trapezoidal, linear interpolation rule using mean concentrations and nominal times. The terminal elimination rate ( $\lambda_z$ ) and half-life ( $HL_{\lambda_z}$ ) was determined using the default “Best Fit” method. The predicted AUC from the last time point to infinity (AUCINF\_pred) was calculated as  $AUC_{last} + C_{last}(pred)/\lambda_z$ .

### In vivo LPS challenge model

Female C57BL/6J mice (Jackson Laboratory) were treated i.p. with TSI-13-57 formulated in 5% NMP, 5% Solutol HS 15, 90% normal saline or vehicle control. 60 min later, the mice were i.p. administered with 2500 ng/kg body weight LPS in PBS. 90 min later, mice were bled and plasma TNF $\alpha$  concentrations were analyzed by ELISA (eBioscience).

### Statistics

Author Manuscript

Statistical analyses were performed using GraphPad Prism 7 software. Pairwise comparisons were analyzed with the Mann-Whitney U test or Paired t test (two-tailed). Multiple comparisons were analyzed by one way or two-way analysis of variance (ANOVA) followed by post-tests.

### Supplementary Material

Refer to Web version on PubMed Central for supplementary material.

### Acknowledgments:

We gratefully acknowledge the staff of the Animal Resource Center at the St. Jude Children’s Research Hospital and the Centers of the Department of Chemical Biology and Therapeutics. We also thank Drs. Li Tang and Yilun Sun (St. Jude Children’s Research Hospital) for support with statistical analyses, and Dr. Ruiqiong Wu for technical contributions.

**Funding:** This work was supported by the National Institutes of Health (PHS 5R01 DK015556 to JAK and T32ES007326 to JAP), the St. Jude Children’s Infection Defense Center (CIDC) and the American Lebanese Syrian Associated Charities (ALSAC).

## REFERENCES AND NOTES

1. Kawai T, Akira S, The role of pattern-recognition receptors in innate immunity: update on Toll-like receptors. *Nature immunology* 11, 373–384 (2010). [PubMed: 20404851]
2. Kumar H, Kawai T, Akira S, Toll-like receptors and innate immunity. *Biochemical and biophysical research communications* 388, 621–625 (2009). [PubMed: 19686699]
3. Foster SL, Medzhitov R, Gene-specific control of the TLR-induced inflammatory response. *Clinical immunology* 130, 7–15 (2009). [PubMed: 18964303]
4. Medzhitov R, Origin and physiological roles of inflammation. *Nature* 454, 428–435 (2008). [PubMed: 18650913]
5. Poltorak A, He X, Smirnova I, Liu MY, Van Huffel C, Du X, Birdwell D, Alejos E, Silva M, Galanos C, Freudenberg M, Ricciardi-Castagnoli P, Layton B, Beutler B, Defective LPS signaling in C3H/HeJ and C57BL/10ScCr mice: mutations in Tlr4 gene. *Science* 282, 2085–2088 (1998). [PubMed: 9851930]
6. Knapp S, Update on the role of Toll-like receptors during bacterial infections and sepsis. *Wiener medizinische Wochenschrift* 160, 107–111 (2010). [PubMed: 20364412]
7. Vilahur G, Badimon L, Ischemia/reperfusion activates myocardial innate immune response: the key role of the toll-like receptor. *Frontiers in physiology* 5, 496 (2014). [PubMed: 25566092]
8. Joosten LA, Abdollahi-Roodsaz S, Dinarello CA, O'Neill L, Netea MG, Toll-like receptors and chronic inflammation in rheumatic diseases: new developments. *Nature reviews. Rheumatology* 12, 344–357 (2016). [PubMed: 27170508]
9. Tall AR, Yvan-Charvet L, Cholesterol, inflammation and innate immunity. *Nature reviews. Immunology* 15, 104–116 (2015).
10. Gay NJ, Keith FJ, Drosophila Toll and IL-1 receptor. *Nature* 351, 355–356 (1991). [PubMed: 1851964]
11. Wesche H, Henzel WJ, Shillinglaw W, Li S, Cao Z, MyD88: an adapter that recruits IRAK to the IL-1 receptor complex. *Immunity* 7, 837–847 (1997). [PubMed: 9430229]
12. Adachi O, Kawai T, Takeda K, Matsumoto M, Tsutsui H, Sakagami M, Nakanishi K, Akira S, Targeted disruption of the MyD88 gene results in loss of IL-1- and IL-18-mediated function. *Immunity* 9, 143–150 (1998). [PubMed: 9697844]
13. He Y, Hara H, Nunez G, Mechanism and Regulation of NLRP3 Inflammasome Activation. *Trends in biochemical sciences* 41, 1012–1021 (2016). [PubMed: 27669650]
14. Chen CJ, Shi Y, Hearn A, Fitzgerald K, Golenbock D, Reed G, Akira S, Rock KL, MyD88-dependent IL-1 receptor signaling is essential for gouty inflammation stimulated by monosodium urate crystals. *The Journal of clinical investigation* 116, 2262–2271 (2006). [PubMed: 16886064]
15. Martinon F, Petrilli V, Mayor A, Tardivel A, Tschopp J, Gout-associated uric acid crystals activate the NALP3 inflammasome. *Nature* 440, 237–241 (2006). [PubMed: 16407889]
16. Pope RM, Tschopp J, The role of interleukin-1 and the inflammasome in gout: implications for therapy. *Arthritis and rheumatism* 56, 3183–3188 (2007). [PubMed: 17907163]
17. Achek A, Yesudhas D, Choi S, Toll-like receptors: promising therapeutic targets for inflammatory diseases. *Archives of pharmacal research* 39, 1032–1049 (2016). [PubMed: 27515048]
18. Muzio M, Ni J, Feng P, Dixit VM, IRAK (Pelle) family member IRAK-2 and MyD88 as proximal mediators of IL-1 signaling. *Science* 278, 1612–1615 (1997). [PubMed: 9374458]
19. Medzhitov R, Preston-Hurlburt P, Kopp E, Stadlen A, Chen C, Ghosh S, Janeway CA Jr., MyD88 is an adaptor protein in the hToll/IL-1 receptor family signaling pathways. *Molecular cell* 2, 253–258 (1998). [PubMed: 9734363]
20. Yamamoto M, Sato S, Hemmi H, Sanjo H, Uematsu S, Kaisho T, Hoshino K, Takeuchi O, Kobayashi M, Fujita T, Takeda K, Akira S, Essential role for TIRAP in activation of the signalling cascade shared by TLR2 and TLR4. *Nature* 420, 324–329 (2002). [PubMed: 12447441]
21. Fitzgerald KA, Palsson-McDermott EM, Bowie AG, Jefferies CA, Mansell AS, Brady G, Brint E, Dunne A, Gray P, Harte MT, McMurray D, Smith DE, Sims JE, Bird TA, O'Neill LA, Mal (MyD88-adaptor-like) is required for Toll-like receptor-4 signal transduction. *Nature* 413, 78–83 (2001). [PubMed: 11544529]

22. Horng T, Barton GM, Medzhitov R, TIRAP: an adapter molecule in the Toll signaling pathway. *Nature immunology* 2, 835–841 (2001). [PubMed: 11526399]
23. Yamamoto M, Sato S, Hemmi H, Hoshino K, Kaisho T, Sanjo H, Takeuchi O, Sugiyama M, Okabe M, Takeda K, Akira S, Role of adaptor TRIF in the MyD88-independent toll-like receptor signaling pathway. *Science* 301, 640–643 (2003). [PubMed: 12855817]
24. Oshiumi H, Matsumoto M, Funami K, Akazawa T, Seya T, TICAM-1, an adaptor molecule that participates in Toll-like receptor 3-mediated interferon-beta induction. *Nature immunology* 4, 161–167 (2003). [PubMed: 12539043]
25. Oshiumi H, Sasai M, Shida K, Fujita T, Matsumoto M, Seya T, TIR-containing adapter molecule (TICAM)-2, a bridging adapter recruiting to toll-like receptor 4 TICAM-1 that induces interferon-beta. *The Journal of biological chemistry* 278, 49751–49762 (2003). [PubMed: 14519765]
26. Fitzgerald KA, Rowe DC, Barnes BJ, Caffrey DR, Visintin A, Latz E, Monks B, Pitha PM, Golenbock DT, LPS-TLR4 signaling to IRF-3/7 and NF-kappaB involves the toll adapters TRAM and TRIF. *The Journal of experimental medicine* 198, 1043–1055 (2003). [PubMed: 14517278]
27. Yamamoto M, Sato S, Hemmi H, Uematsu S, Hoshino K, Kaisho T, Takeuchi O, Takeda K, Akira S, TRAM is specifically involved in the Toll-like receptor 4-mediated MyD88-independent signaling pathway. *Nature immunology* 4, 1144–1150 (2003). [PubMed: 14556004]
28. Kawai T, Adachi O, Ogawa T, Takeda K, Akira S, Unresponsiveness of MyD88-deficient mice to endotoxin. *Immunity* 11, 115–122 (1999). [PubMed: 10435584]
29. Lin SC, Lo YC, Wu H, Helical assembly in the MyD88-IRAK4-IRAK2 complex in TLR/IL-1R signalling. *Nature* 465, 885–890 (2010). [PubMed: 20485341]
30. Hacker H, Redecke V, Blagoev B, Kratchmarova I, Hsu LC, Wang GG, Kamps MP, Raz E, Wagner H, Hacker G, Mann M, Karin M, Specificity in Toll-like receptor signalling through distinct effector functions of TRAF3 and TRAF6. *Nature* 439, 204–207 (2006). [PubMed: 16306937]
31. Cao Z, Xiong J, Takeuchi M, Kurama T, Goeddel DV, TRAF6 is a signal transducer for interleukin-1. *Nature* 383, 443–446 (1996). [PubMed: 8837778]
32. Gohda J, Matsumura T, Inoue J, Cutting edge: TNFR-associated factor (TRAF) 6 is essential for MyD88-dependent pathway but not toll/IL-1 receptor domain-containing adaptor-inducing IFN-beta (TRIF)-dependent pathway in TLR signaling. *Journal of immunology* 173, 2913–2917 (2004).
33. Walsh MC, Lee J, Choi Y, Tumor necrosis factor receptor-associated factor 6 (TRAF6) regulation of development, function, and homeostasis of the immune system. *Immunological reviews* 266, 72–92 (2015). [PubMed: 26085208]
34. von Bernuth H, Picard C, Puel A, Casanova JL, Experimental and natural infections in MyD88- and IRAK-4-deficient mice and humans. *European journal of immunology* 42, 3126–3135 (2012). [PubMed: 23255009]
35. Zhou J, Wu R, High AA, Slaughter CA, Finkelstein D, Rehg JE, Redecke V, Hacker H, A20-binding inhibitor of NF-kappaB (ABIN1) controls Toll-like receptor-mediated CCAAT/enhancer-binding protein beta activation and protects from inflammatory disease. *Proceedings of the National Academy of Sciences of the United States of America* 108, E998–1006 (2011). [PubMed: 22011580]
36. Farrar MA, Alberol-Ila J, Perlmutter RM, Activation of the Raf-1 kinase cascade by coumermycin-induced dimerization. *Nature* 383, 178–181 (1996). [PubMed: 8774884]
37. Horng T, Barton GM, Flavell RA, Medzhitov R, The adaptor molecule TIRAP provides signalling specificity for Toll-like receptors. *Nature* 420, 329–333 (2002). [PubMed: 12447442]
38. Hideshima T, Chauhan D, Richardson P, Mitsiades C, Mitsiades N, Hayashi T, Munshi N, Dang L, Castro A, Palombella V, Adams J, Anderson KC, NF-kappa B as a therapeutic target in multiple myeloma. *The Journal of biological chemistry* 277, 16639–16647 (2002). [PubMed: 11872748]
39. Hacker H, Karin M, Regulation and function of IKK and IKK-related kinases. *Science's STKE : signal transduction knowledge environment* 2006, re13 (2006).
40. Karaman MW, Herrgard S, Treiber DK, Gallant P, Atteridge CE, Campbell BT, Chan KW, Ciceri P, Davis MI, Edeen PT, Faraoni R, Floyd M, Hunt JP, Lockhart DJ, Milanov ZV, Morrison MJ, Pallares G, Patel HK, Pritchard S, Wodicka LM, Zarrinkar PP, A quantitative analysis of kinase inhibitor selectivity. *Nature biotechnology* 26, 127–132 (2008).

41. Hacker H, Vabulas RM, Takeuchi O, Hoshino K, Akira S, Wagner H, Immune cell activation by bacterial CpG-DNA through myeloid differentiation marker 88 and tumor necrosis factor receptor-associated factor (TRAF)6. *The Journal of experimental medicine* 192, 595–600 (2000). [PubMed: 10952730]
42. Taylor PR, Tsoni SV, Willment JA, Dennehy KM, Rosas M, Findon H, Haynes K, Steele C, Botto M, Gordon S, Brown GD, Dectin-1 is required for beta-glucan recognition and control of fungal infection. *Nature immunology* 8, 31–38 (2007). [PubMed: 17159984]
43. Sun J, Huang YR, Harrington WR, Sheng S, Katzenellenbogen JA, Katzenellenbogen BS, Antagonists selective for estrogen receptor alpha. *Endocrinology* 143, 941–947 (2002). [PubMed: 11861516]
44. Suzuki N, Suzuki S, Duncan GS, Millar DG, Wada T, Mirtsos C, Takada H, Wakeham A, Itie A, Li S, Penninger JM, Wesche H, Ohashi PS, Mak TW, Yeh WC, Severe impairment of interleukin-1 and Toll-like receptor signalling in mice lacking IRAK-4. *Nature* 416, 750–756 (2002). [PubMed: 11923871]
45. Li S, Strelow A, Fontana EJ, Wesche H, IRAK-4: a novel member of the IRAK family with the properties of an IRAK-kinase. *Proceedings of the National Academy of Sciences of the United States of America* 99, 5567–5572 (2002). [PubMed: 11960013]
46. Burns K, Martinon F, Esslinger C, Pahl H, Schneider P, Bodmer JL, Di Marco F, French L, Tschopp J, MyD88, an adapter protein involved in interleukin-1 signaling. *The Journal of biological chemistry* 273, 12203–12209 (1998). [PubMed: 9575168]
47. Stauffer SR, Huang YR, Aron ZD, Coletta CJ, Sun J, Katzenellenbogen BS, Katzenellenbogen JA, Triarylpyrazoles with basic side chains: development of pyrazole-based estrogen receptor antagonists. *Bioorganic & medicinal chemistry* 9, 151–161 (2001). [PubMed: 11197335]
48. Stauffer SR, Huang Y, Coletta CJ, Tedesco R, Katzenellenbogen JA, Estrogen pyrazoles: defining the pyrazole core structure and the orientation of substituents in the ligand binding pocket of the estrogen receptor. *Bioorganic & medicinal chemistry* 9, 141–150 (2001). [PubMed: 11197334]
49. Stauffer SR, Coletta CJ, Tedesco R, Nishiguchi G, Carlson K, Sun J, Katzenellenbogen BS, Katzenellenbogen JA, Pyrazole ligands: structure-affinity/activity relationships and estrogen receptor-alpha-selective agonists. *Journal of medicinal chemistry* 43, 4934–4947 (2000). [PubMed: 11150164]
50. Pfeffer K, Matsuyama T, Kundig TM, Wakeham A, Kishihara K, Shahinian A, Wiegmann K, Ohashi PS, Kronke M, Mak TW, Mice deficient for the 55 kd tumor necrosis factor receptor are resistant to endotoxic shock, yet succumb to *L. monocytogenes* infection. *Cell* 73, 457–467 (1993). [PubMed: 8387893]
51. Snyder GA, Cirl C, Jiang J, Chen K, Waldhuber A, Smith P, Rommler F, Snyder N, Fresquez T, Durr S, Tjandra N, Miethke T, Xiao TS, Molecular mechanisms for the subversion of MyD88 signaling by TcpC from virulent uropathogenic *Escherichia coli*. *Proceedings of the National Academy of Sciences of the United States of America* 110, 6985–6990 (2013). [PubMed: 23569230]
52. Li C, Zienkiewicz J, Hawiger J, Interactive sites in the MyD88 Toll/interleukin (IL) 1 receptor domain responsible for coupling to the IL1beta signaling pathway. *The Journal of biological chemistry* 280, 26152–26159 (2005). [PubMed: 15849357]
53. Loiarro M, Capolunghi F, Fanto N, Gallo G, Campo S, Arseni B, Carsetti R, Carminati P, De Santis R, Ruggiero V, Sette C, Pivotal Advance: Inhibition of MyD88 dimerization and recruitment of IRAK1 and IRAK4 by a novel peptidomimetic compound. *Journal of leukocyte biology* 82, 801–810 (2007). [PubMed: 17548806]
54. Mistry P, Laird MH, Schwarz RS, Greene S, Dyson T, Snyder GA, Xiao TS, Chauhan J, Fletcher S, Toshchakov VY, MacKerell AD Jr., Vogel SN, Inhibition of TLR2 signaling by small molecule inhibitors targeting a pocket within the TLR2 TIR domain. *Proceedings of the National Academy of Sciences of the United States of America* 112, 5455–5460 (2015). [PubMed: 25870276]
55. Cushing L, Stochaj W, Siegel M, Czerwinski R, Dower K, Wright Q, Hirschfield M, Casanova JL, Picard C, Puel A, Lin LL, Rao VR, Interleukin 1/Toll-like receptor-induced autophosphorylation activates interleukin 1 receptor-associated kinase 4 and controls cytokine induction in a cell type-specific manner. *The Journal of biological chemistry* 289, 10865–10875 (2014). [PubMed: 24567333]

56. Koziczak-Holbro M, Joyce C, Gluck A, Kinzel B, Muller M, Tschopp C, Mathison JC, Davis CN, Gram H, IRAK-4 kinase activity is required for interleukin-1 (IL-1) receptor- and toll-like receptor 7-mediated signaling and gene expression. *The Journal of biological chemistry* 282, 13552–13560 (2007). [PubMed: 17337443]
57. Kim TW, Staschke K, Bulek K, Yao J, Peters K, Oh KH, Vandenburg Y, Xiao H, Qian W, Hamilton T, Min B, Sen G, Gilmour R, Li X, A critical role for IRAK4 kinase activity in Toll-like receptor-mediated innate immunity. *The Journal of experimental medicine* 204, 1025–1036 (2007). [PubMed: 17470642]
58. Kawagoe T, Sato S, Jung A, Yamamoto M, Matsui K, Kato H, Uematsu S, Takeuchi O, Akira S, Essential role of IRAK-4 protein and its kinase activity in Toll-like receptor-mediated immune responses but not in TCR signaling. *The Journal of experimental medicine* 204, 1013–1024 (2007). [PubMed: 17485511]
59. Wang Z, Liu J, Sudom A, Ayres M, Li S, Wesche H, Powers JP, Walker NP, Crystal structures of IRAK-4 kinase in complex with inhibitors: a serine/threonine kinase with tyrosine as a gatekeeper. *Structure* 14, 1835–1844 (2006). [PubMed: 17161373]
60. Powers JP, Li S, Jaen JC, Liu J, Walker NP, Wang Z, Wesche H, Discovery and initial SAR of inhibitors of interleukin-1 receptor-associated kinase-4. *Bioorganic & medicinal chemistry letters* 16, 2842–2845 (2006). [PubMed: 16563752]
61. Wang Z, Sun D, Johnstone S, Cao Z, Gao X, Jaen JC, Liu J, Lively S, Miao S, Sudom A, Tomooka C, Walker NP, Wright M, Yan X, Ye Q, Powers JP, Discovery of potent, selective, and orally bioavailable inhibitors of interleukin-1 receptor-associated kinase-4. *Bioorganic & medicinal chemistry letters* 25, 5546–5550 (2015). [PubMed: 26526214]
62. Buckley GM, Ceska TA, Fraser JL, Gowers L, Groom CR, Higuieruelo AP, Jenkins K, Mack SR, Morgan T, Parry DM, Pitt WR, Rausch O, Richard MD, Sabin V, IRAK-4 inhibitors. Part II: a structure-based assessment of imidazo[1,2-a]pyridine binding. *Bioorganic & medicinal chemistry letters* 18, 3291–3295 (2008). [PubMed: 18482836]
63. Buckley GM, Fosbeary R, Fraser JL, Gowers L, Higuieruelo AP, James LA, Jenkins K, Mack SR, Morgan T, Parry DM, Pitt WR, Rausch O, Richard MD, Sabin V, IRAK-4 inhibitors. Part III: a series of imidazo[1,2-a]pyridines. *Bioorganic & medicinal chemistry letters* 18, 3656–3660 (2008). [PubMed: 18501603]
64. Tumey LN, Boschelli DH, Bhagirath N, Shim J, Murphy EA, Goodwin D, Bennett EM, Wang M, Lin LL, Press B, Shen M, Frisbie RK, Morgan P, Mohan S, Shin J, Rao VR, Identification and optimization of indolo[2,3-c]quinoline inhibitors of IRAK4. *Bioorganic & medicinal chemistry letters* 24, 2066–2072 (2014). [PubMed: 24726805]
65. McElroy WT, Michael Seganish W, Jason Herr R, Harding J, Yang J, Yet L, Komanduri V, Prakash KC, Lavey B, Tulshian D, Greenlee WJ, Sondey C, Fischmann TO, Niu X, Discovery and hit-to-lead optimization of 2,6-diaminopyrimidine inhibitors of interleukin-1 receptor-associated kinase 4. *Bioorganic & medicinal chemistry letters* 25, 1836–1841 (2015). [PubMed: 25870132]
66. McElroy WT, Tan Z, Ho G, Paliwal S, Li G, Seganish WM, Tulshian D, Tata J, Fischmann TO, Sondey C, Bian H, Bober L, Jackson J, Garlisi CG, Devito K, Fossetta J, Lundell D, Niu X, Potent and Selective Amidopyrazole Inhibitors of IRAK4 That Are Efficacious in a Rodent Model of Inflammation. *ACS medicinal chemistry letters* 6, 677–682 (2015). [PubMed: 26101573]
67. Lim J, Altman MD, Baker J, Brubaker JD, Chen H, Chen Y, Fischmann T, Gibeau C, Kleinschek MA, Leccese E, Lesburg C, Maclean JK, Moy LY, Mulrooney EF, Presland J, Rakhilina L, Smith GF, Steinhuebel D, Yang R, Discovery of 5-Amino-N-(1H-pyrazol-4-yl)pyrazolo[1,5-a]pyrimidine-3-carboxamide Inhibitors of IRAK4. *ACS medicinal chemistry letters* 6, 683–688 (2015). [PubMed: 26101574]
68. Kelly PN, Romero DL, Yang Y, Shaffer AL 3rd, Chaudhary D, Robinson S, Miao W, Rui L, Westlin WF, Kapeller R, Staudt LM, Selective interleukin-1 receptor-associated kinase 4 inhibitors for the treatment of autoimmune disorders and lymphoid malignancy. *The Journal of experimental medicine* 212, 2189–2201 (2015). [PubMed: 26621451]
69. Lee KL, Ambler CM, Anderson DR, Boscoe BP, Bree AG, Brodfuehrer JI, Chang JS, Choi C, Chung S, Curran KJ, Day JE, Dehnhardt CM, Dower K, Drozda SE, Frisbie RK, Gavrin LK, Goldberg JA, Han S, Hegen M, Hepworth D, Hope HR, Kamtekar S, Kilty IC, Lee A, Lin LL, Lovering FE, Lowe MD, Mathias JP, Morgan HM, Murphy EA, Papaioannou N, Patny A, Pierce

- BS, Rao VR, Saiah E, Samardjiev IJ, Samas BM, Shen MWH, Shin JH, Soutter HH, Strohbach JW, Symanowicz PT, Thomason JR, Trzuppek JD, Vargas R, Vincent F, Yan J, Zapf CW, Wright SW, Discovery of Clinical Candidate 1-[[[(2S,3S,4S)-3-Ethyl-4-fluoro-5-oxopyrrolidin-2-yl]methoxy]-7-methoxyisoquinoline-6-carboxamide (PF-06650833), a Potent, Selective Inhibitor of Interleukin-1 Receptor Associated Kinase 4 (IRAK4), by Fragment-Based Drug Design. *Journal of medicinal chemistry* 60, 5521–5542 (2017). [PubMed: 28498658]
70. Celhar T, Magalhaes R, Fairhurst AM, TLR7 and TLR9 in SLE: when sensing self goes wrong. *Immunologic research* 53, 58–77 (2012). [PubMed: 22434514]
71. Hacker H, Mischak H, Hacker G, Eser S, Prenzel N, Ullrich A, Wagner H, Cell type-specific activation of mitogen-activated protein kinases by CpG-DNA controls interleukin-12 release from antigen-presenting cells. *The EMBO journal* 18, 6973–6982 (1999). [PubMed: 10601019]
72. Lubahn DB, Moyer JS, Golding TS, Couse JF, Korach KS, Smithies O, Alteration of reproductive function but not prenatal sexual development after insertional disruption of the mouse estrogen receptor gene. *Proceedings of the National Academy of Sciences of the United States of America* 90, 11162–11166 (1993). [PubMed: 8248223]
73. Redecke V, Wu R, Zhou J, Finkelstein D, Chaturvedi V, High AA, Hacker H, Hematopoietic progenitor cell lines with myeloid and lymphoid potential. *Nature methods* 10, 795–803 (2013). [PubMed: 23749299]
74. Sanjana NE, Shalem O, Zhang F, Improved vectors and genome-wide libraries for CRISPR screening. *Nature methods* 11, 783–784 (2014). [PubMed: 25075903]
75. Tawaratsumida K, Phan V, Hrincius ER, High AA, Webby R, Redecke V, Hacker H, Quantitative proteomic analysis of the influenza A virus nonstructural proteins NS1 and NS2 during natural cell infection identifies PACT as an NS1 target protein and antiviral host factor. *Journal of virology* 88, 9038–9048 (2014). [PubMed: 24899174]
76. Cox J, Mann M, MaxQuant enables high peptide identification rates, individualized p.p.b.-range mass accuracies and proteome-wide protein quantification. *Nature biotechnology* 26, 1367–1372 (2008).
77. Carlson KE, Choi I, Gee A, Katzenellenbogen BS, Katzenellenbogen JA, Altered ligand binding properties and enhanced stability of a constitutively active estrogen receptor: evidence that an open pocket conformation is required for ligand interaction. *Biochemistry* 36, 14897–14905 (1997). [PubMed: 9398213]
78. Jafari R, Almquist H, Axelsson H, Ignatushchenko M, Lundback T, Nordlund P, Martinez Molina D, The cellular thermal shift assay for evaluating drug target interactions in cells. *Nature protocols* 9, 2100–2122 (2014). [PubMed: 25101824]
79. Zhang JH, Chung TD, Oldenburg KR, A Simple Statistical Parameter for Use in Evaluation and Validation of High Throughput Screening Assays. *Journal of biomolecular screening* 4, 67–73 (1999). [PubMed: 10838414]
80. Pangborn AB, Giardello MA, Grubbs RH, Rosen RK, Timmers FJ, Safe and convenient procedure for solvent purification. *Organometallics* 15, 1518–1520 (1996).
81. Huang YR, Katzenellenbogen JA, Regioselective synthesis of 1,3,5-triaryl-4-alkylpyrazoles: novel ligands for the estrogen receptor. *Organic letters* 2, 2833–2836 (2000). [PubMed: 10964377]
82. Grice CA, Tays KL, Savall BM, Wei J, Butler CR, Axe FU, Bembenek SD, Fourie AM, Dunford PJ, Lundeen K, Coles F, Xue X, Riley JP, Williams KN, Karlsson L, Edwards JP, Identification of a potent, selective, and orally active leukotriene a4 hydrolase inhibitor with anti-inflammatory activity. *Journal of medicinal chemistry* 51, 4150–4169 (2008). [PubMed: 18588282]

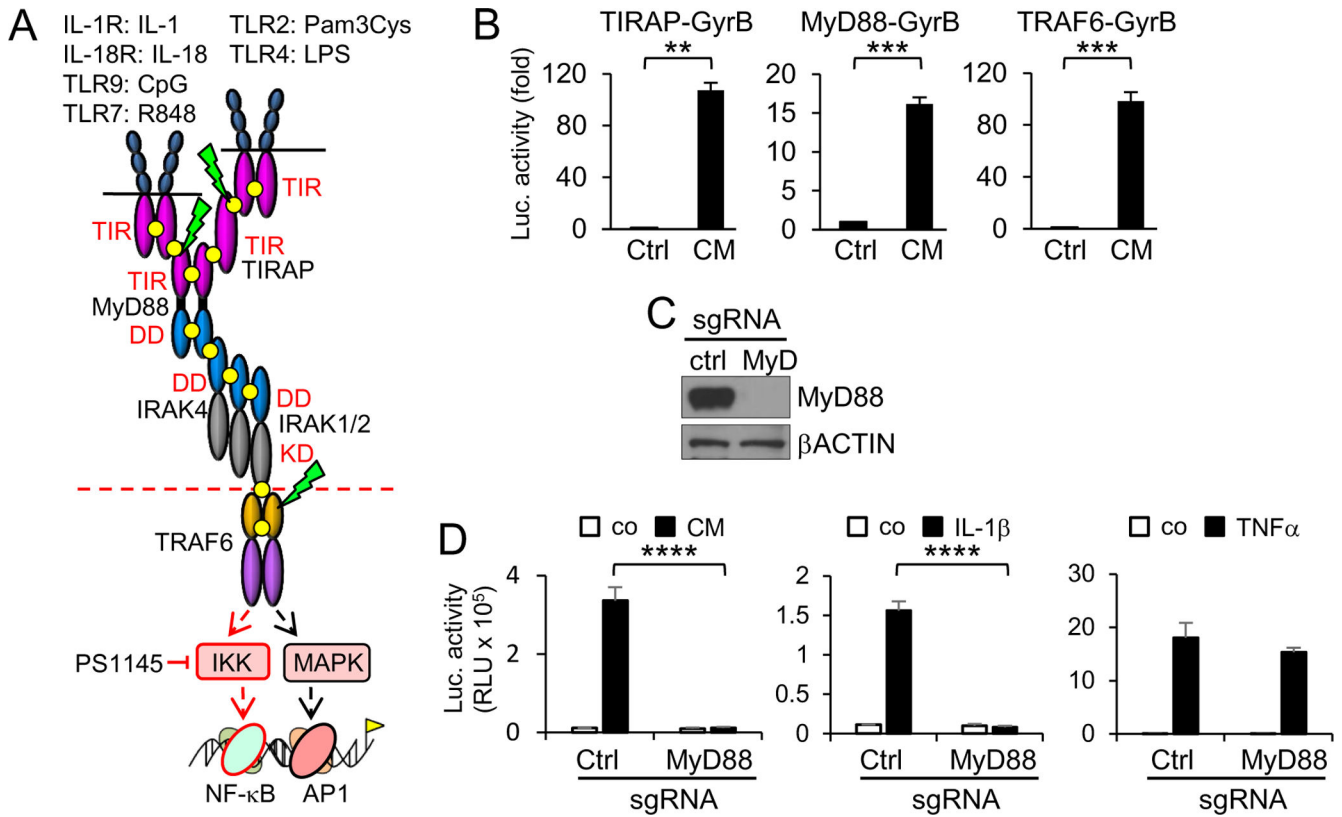


**Fig. 1. A phenotypic HTS platform based on hierarchically acting TLR-signaling proteins.** (A) Model of the MyD88 signaling pathway activated by different TLR and IL-1R family members. Established protein interactions are highlighted (yellow circles). Proteins activated by Coumermycin (CM)-induced GyraseB (GyrB) dimerization are indicated with green bolts. TIR domains are shown in purple, death domains (DD) in dark blue. AP1, activator protein 1. (B) NF-κB luciferase reporter activity in HEK293T cells transfected with the indicated GyrB-fusion proteins and treated as indicated. Fold change data normalized to vehicle-treated controls (Ctrl) are means ± SD from 3 independent experiments. (C) Western blot analysis of MyD88 expression in TIRAP-GyrB-expressing HEK293T cells that were infected with lentivirus expressing CAS9 and control sgRNA (ctrl) or sgRNA against MyD88 (MyD). Blots are representative of 3 independent experiments. (D) NF-κB luciferase reporter activity of TIRAP-GyrB-expressing HEK293T cells transduced with CAS9/indicated sgRNA and stimulated as indicated. Data are means ± SD from 3 independent experiments. \*\*P < 0.01, \*\*\*P < 0.001, \*\*\*\*P < 0.0001 by Mann-Whitney U test (B) or two-way ANOVA with Sidak’s multiple comparison test (D).

Author Manuscript

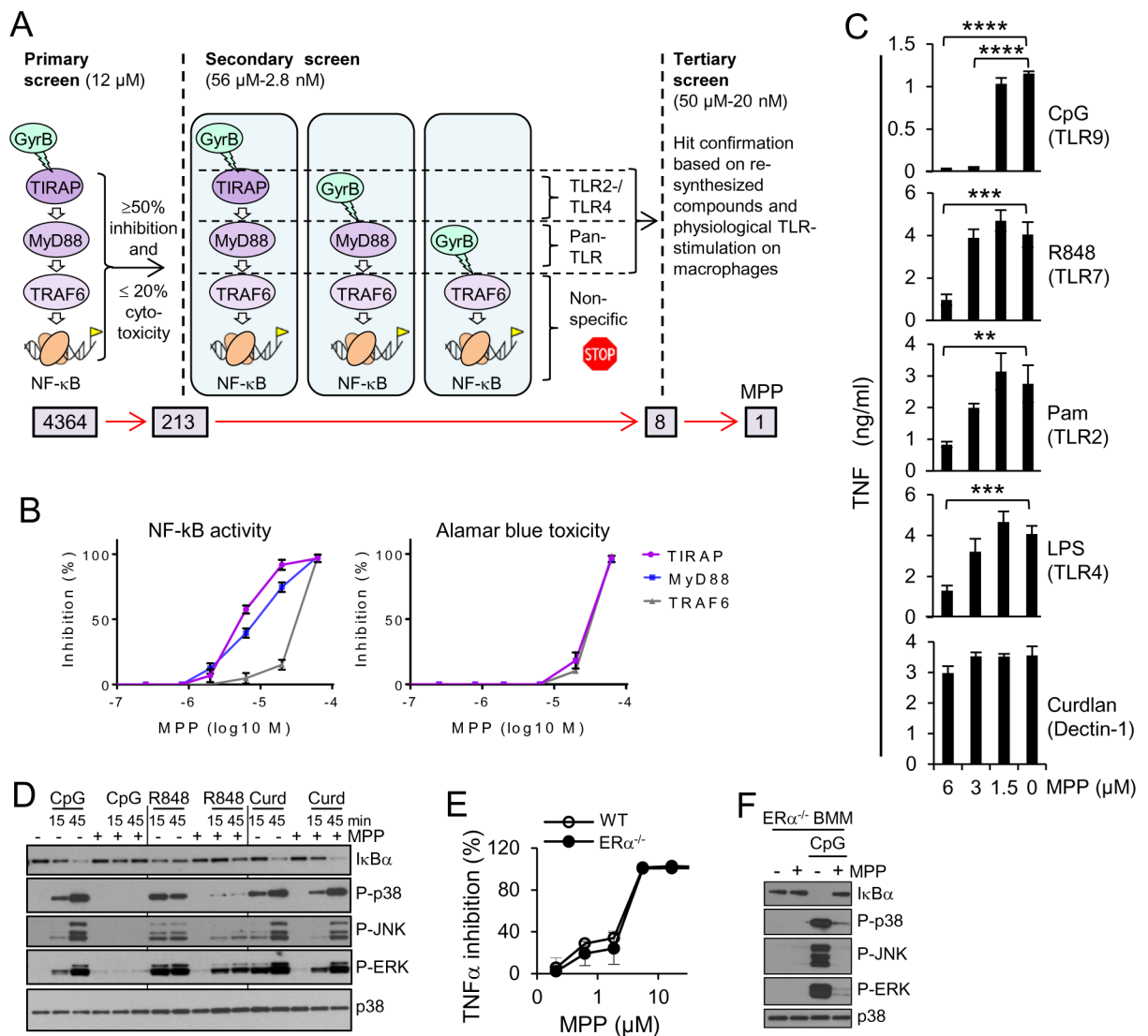


**Fig. 2. Identification of MPP as TLR-inhibitory compound using HTS based on inducible TLR signaling proteins.**

(A) Schematic of HTS workflow. (B) NF- $\kappa$ B luciferase reporter activity (left) and Alamar Blue-determined cell viability (right) for the indicated reporter cell lines after treatment with MPP. Data are means  $\pm$  SD from 3 independent experiments. (C) ELISA analysis of TNF $\alpha$  production by mouse BMM stimulated with TLR agonists for six hours in the presence of the indicated concentration of MPP. Data are means  $\pm$  SD of 3 independent experiments. (D) Western blot analysis of the indicated proteins in lysates from CpG-DNA-, R848- and Curdlan-treated BMM in the presence or absence of MPP. Antibodies against total p38 were used as loading control. Blots are representative of 3 independent experiments. (E) ELISA analysis of TNF $\alpha$  production by wild-type (WT) and ER $\alpha$ -deficient BMM that were treated for six hours with CpG-DNA in the presence of the indicated concentration of MPP. Data are means  $\pm$  SD of 3 independent experiments. (F) Western blot analysis of I $\kappa$ B $\alpha$  and MAPK-phosphorylation in lysates from ER $\alpha$ -deficient BMM that were treated for 20 min with CpG-DNA in the presence or absence of MPP. Antibodies against total p38 were used as



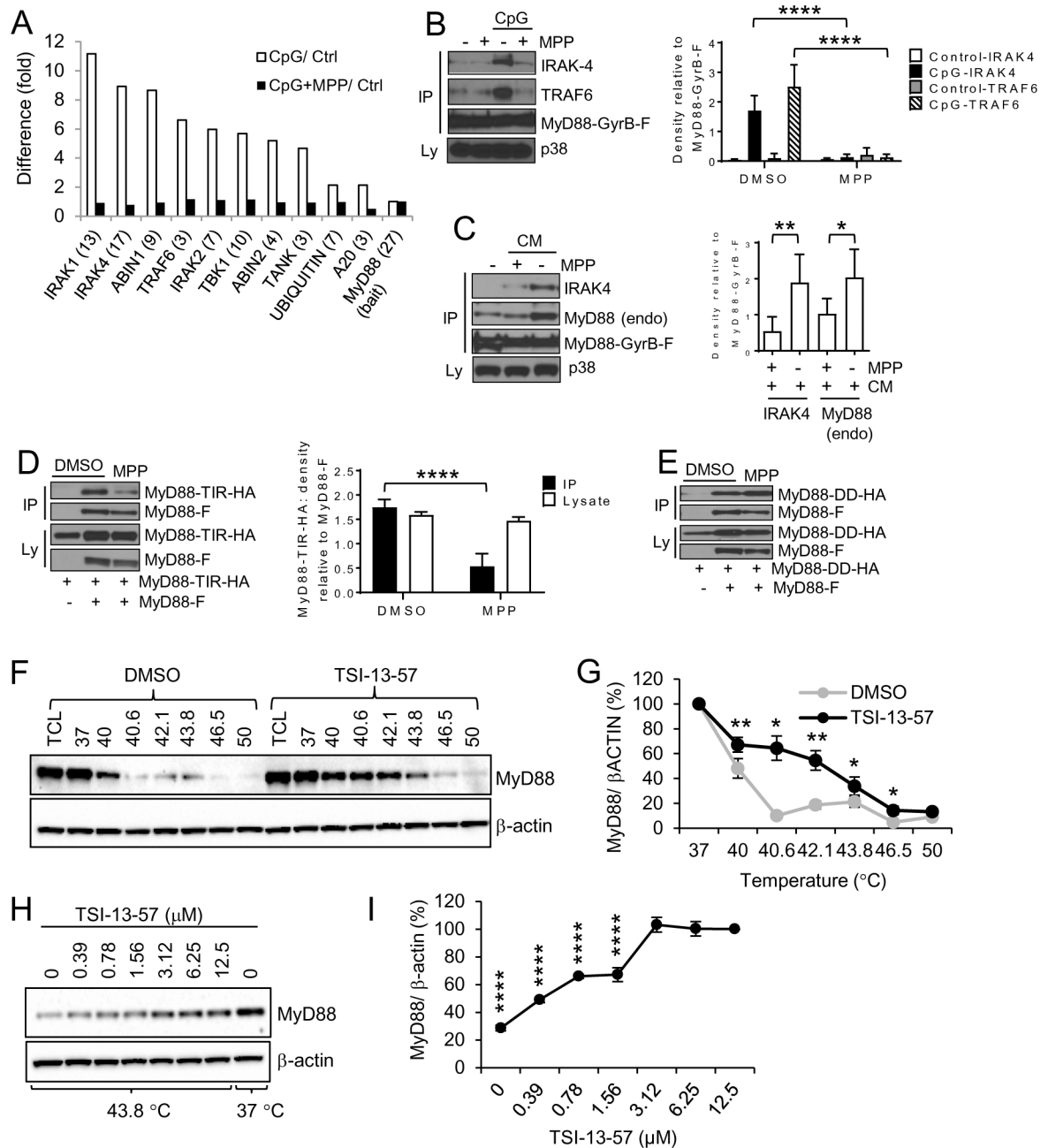
loading control. Blots are representative of 3 independent experiments. \*\*P < 0.01, \*\*\*P < 0.001, \*\*\*\*P < 0.0001 by One-way ANOVA with Dunnett's multiple comparisons test (C), or a Paired t test (two-tailed) (E).

Author Manuscript

Author Manuscript

Author Manuscript

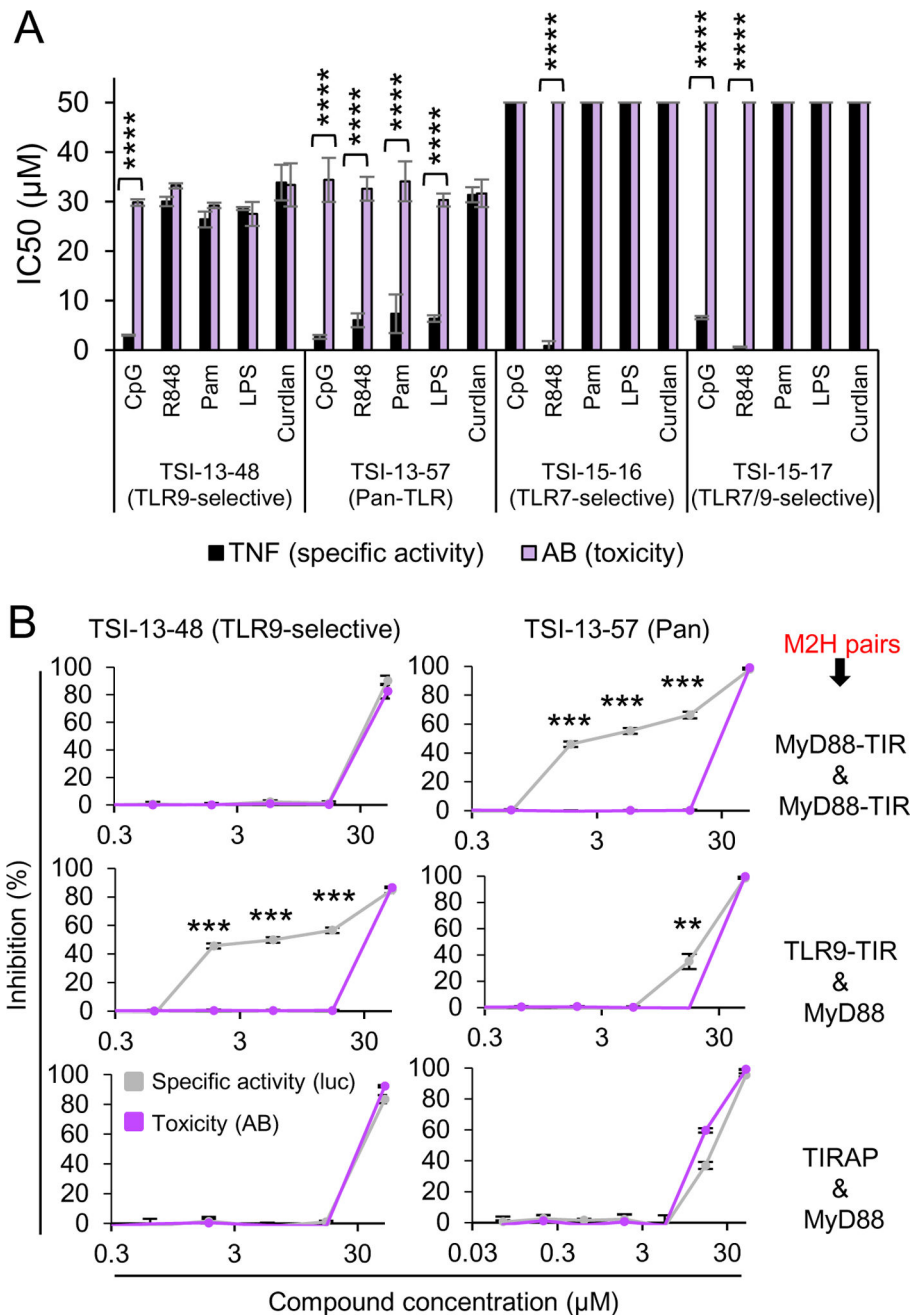
Author Manuscript



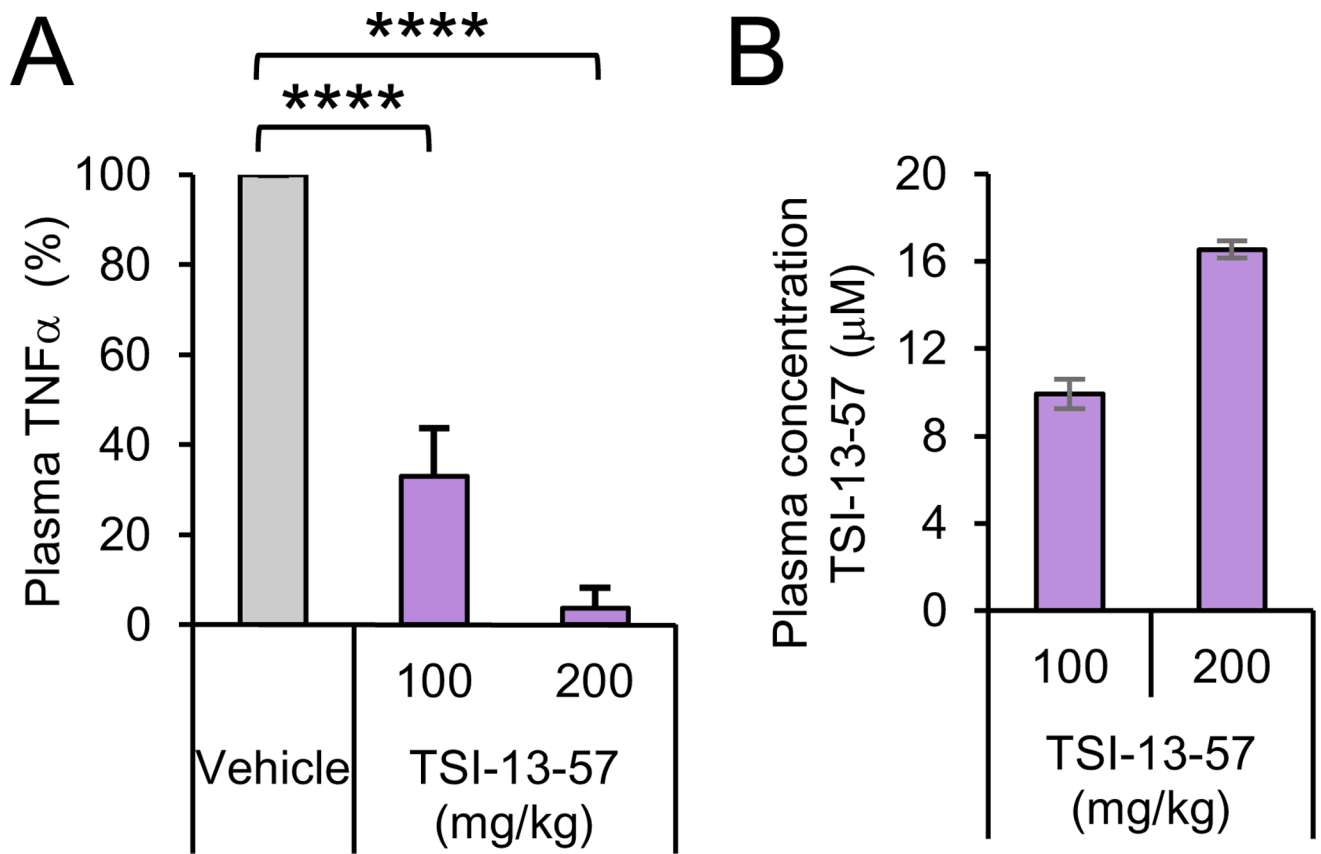
**Fig. 3. TSI blocks formation of the MyD88 signaling complex by interference with TIR-mediated dimerization.**

(A) Quantitative MS analysis of proteins co-purifying with MyD88 in CpG-DNA-stimulated RAW264.7 cells treated with MPP, as indicated. Data are the fold-change in peptide abundance from CpG-DNA-treated vs. control cells (open bars) and CpG-DNA plus MPP-treated vs. control cells (closed bars). Numbers in parenthesis indicate the number of unique peptides identified. (B and C) Western blot analysis and densitometry-based quantification of the indicated proteins co-precipitating with MyD88 in lysates from MyD88-GyrB-F (Flag)-expressing RAW264.7 cells treated with CpG-DNA (45 min) (B) or CM (20 min) (C) and MPP as indicated. Endo = endogenous. Blots are representative of 3 independent

experiments. **(D)** Western blot analysis and densitometry-based quantification of MyD88 domains co-precipitating with MyD88 in lysates from HEK293T cells transfected with full-length (MyD88-F) or TIR-domain (TIR-HA) of MyD88 and treated with MPP, as indicated. Blots are representative of 4 independent experiments. **(E)** Western blot analysis of MyD88 domains co-precipitating with MyD88 in lysates from HEK293T cells transfected with full-length (MyD88-F) or DD-domain of MyD88 and treated with MPP, as indicated. Blots are representative of 4 independent experiments. **(F-I)** Cellular thermal shift assay analysis of the stability of endogenous MyD88 in HEK293T cells exposed to the indicated temperatures and 50  $\mu$ M TSI-13-57 (F, G) or the indicated concentrations of TSI-13-57 and 43.8  $^{\circ}$ C (H, I). Western blots (F, H) are representative of three independent experiments. MyD88 band intensities (G, I) normalized to  $\beta$ -ACTIN relative to controls (37 $^{\circ}$ C (G); 12.5  $\mu$ M (I)) are means  $\pm$  SD pooled from three independent experiments. \*P < 0.05, \*\*P < 0.01, \*\*\*\*P < 0.0001 by two-way ANOVA with Sidak's multiple comparison test (B, D) or One-way ANOVA with Sidak's multiple comparison test (C) or Paired t test (two-tailed) (G) or One-way ANOVA with Dunett's multiple comparisons test (I)..



**Fig. 4. MPP analogs with selectivity against specific TLRs signaling pathways and TIR domains.** (A) ELISA analysis of TNF $\alpha$  production and Alamar blue staining for cell viability in RAW264.7 cells treated as indicated. Data are mean IC<sub>50</sub> values  $\pm$  SD from 3 independent experiments. (B) Interaction-dependent luciferase activity and cell toxicity in HEK293T cells transfected with the indicated mammalian two-hybrid (M2H) protein pairs and a Gal4 luciferase reporter treated with TSI-13-48 and TSI-13-57 at indicated concentrations. Data relative to maximal inhibition by staurosporine are means  $\pm$  SD from 3 independent experiments. \*\*P < 0.01, \*\*\*P < 0.001, \*\*\*\*P < 0.0001 by two-way ANOVA with Sidak's multiple comparison test (A) or Paired t test (two-tailed) (B).

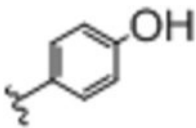
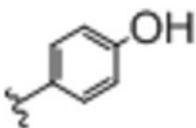
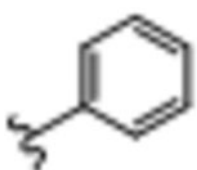
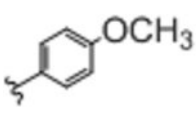
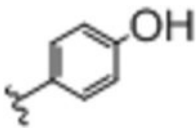
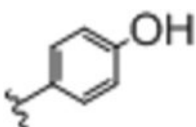


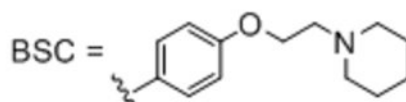
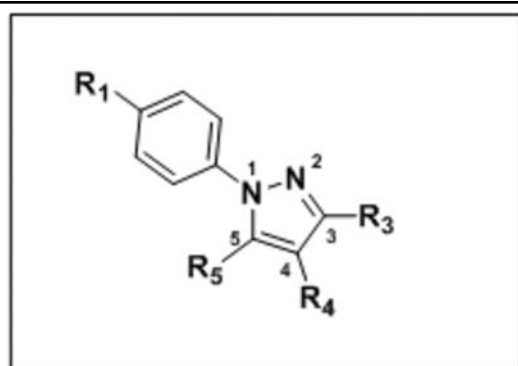
**Fig. 5. TSI-13-57-mediated inhibition of LPS-induced TNF $\alpha$  release in vivo.**

(A) ELISA analysis of TNF $\alpha$  concentration in the plasma of mice that were pre-treated as indicated and challenged with i.p. LPS. Data relative to vehicle control treatment are means  $\pm$  SD of 5 mice per group from 2 independent experiments. (B) LC-MS/MS analysis of TSI-13-57 concentration in the plasma of mice described in (A). Data are means  $\pm$  SD of 5 mice per group from 2 independent experiments \*\*\*\*P < 0.0001 by One-way ANOVA with Dunnett's multiple comparisons test (A).

**Table 1.**  
**Initial SAR to differentiate TLR inhibition from ER binding affinity.**

IC<sub>50</sub> and EC<sub>50</sub> values for TLR9 were obtained using RAW264.7 cells. Values are presented as mean ± SD of three independent experiments.

Entry	Compound	R <sub>1</sub>	R <sub>3</sub>	R <sub>4</sub>	R <sub>5</sub>	TLR9 IC <sub>50</sub> (μM)	TLR9 Toxicity EC <sub>50</sub> (μM)	RF ER
1	MPP	OH		CH <sub>3</sub>	BSC	2.11 ± 0.64	13.2 ± 2.4	12
2	TSI-13-03	OH		Et		32.1 ± 1.43	43 ± 6.4	8.9 0.5
3	TSI-13-30	OCH <sub>3</sub>		CH <sub>3</sub>	BSC	1.97 ± 1.72	33.2 ± 2.7	0.0 ± 0.0
4	TSI-13-27	OH		H	BSC	1.03 ± 0.8	12.3 ± 3.7	5.9 0.1
5	TSI-13-04	OH		Et	BSC	2.84 ± 0.12	11.6 ± 0.9	11 1.5



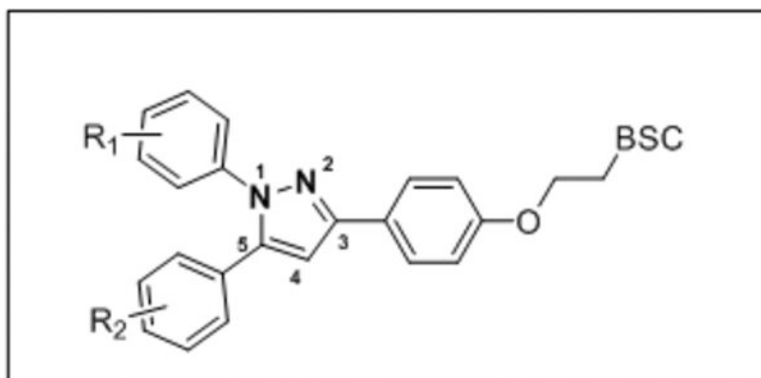
Entry	Compound	R <sub>1</sub>	R <sub>3</sub>	R <sub>4</sub>	R <sub>5</sub>	TLR9 IC <sub>50</sub> (μM)	TLR9 Toxicity EC <sub>50</sub> (μM)	RBA EC <sub>50</sub>
6	TSI-13-19	OH			BSC	28.2 ± 0.5	35.7 ± 4.7	17.5 ± 5.1
7	TSI-13-06	OH		BSC	Et	3.12 ± 0.103	11.2 ± 1.1	7.3 ± 0.0
8	TSI-13-07	OH		BSC	<i>n</i> -Pr	2.96 ± 0.2	12.9 ± 0.3	8.5 ± 2.1
9	TSI-13-05	OH	BSC	Et		3.33 ± 0.2	7.4 ± 0.4	0.1

<sup>a</sup>RBA = relative binding affinity values, where estradiol = 100.

<sup>b</sup>Single determinations.

**Table 2.**  
**Initial hit compounds that demonstrate selective TLR inhibition.**

IC<sub>50</sub> and EC<sub>50</sub> values were obtained using RAW264.7 cells. n.d., not done. Values are presented as mean ± SD of three independent experiments.



Entry	Compound	R <sub>1</sub>	R <sub>2</sub>	BSC	IC <sub>50</sub> (μM) TLR9	TLR7	TLR2	TLR4	EC <sub>50</sub> (μM) Toxicity
1	TSI-13-50	<i>p</i> -OH	H	1- piperidinyl	6.82 ± 0.65	15.6 ± 1.0	8.11 ± 2.19	15.8 ± 3.1	21.4 ± 5.2
2	TSI-13-60	OH	<i>p</i> -OH	1- piperidinyl	3.04 ± 1.37	2.07 ± 0.62	5.9 ± 1.97	5.56 ± 0.64	33.8 ± 2.6
3	TSI-13-57	<i>p</i> -OH	<i>p</i> -OH	1- piperidinyl	2.7 ± 0.39	6.03 ± 1.41	7.37 ± 3.88	6.38 ± 0.66	32.6 ± 3.2
4	TSI-13-58	<i>p</i> -OH	<i>m</i> -OH	1- piperidinyl	30.2 ± 0.1	n.d.	50	n.d.	50
5	TSI-13-48	<i>p</i> -NO <sub>2</sub>	<i>p</i> -OCH <sub>3</sub>	1- piperidinyl	3.02 ± 0.11	30.0 ± 0.9	26.4 ± 1.6	28.6 ± 0.3	30.6 ± 3.1
6	TSI-14-44	<i>p</i> -OCH <sub>3</sub>	3,4,5-(OCH <sub>3</sub> ) <sub>3</sub>	1- piperidinyl	3.43 ± 0.49	2.24 ± 0.63	2.28 ± 1.10	1.15 ± 0.39	14.6 ± 0.1
7	TSI-15-17	H	5-OCH <sub>3</sub> -3,4- dioxymethylene	1- piperidinyl	6.59 ± 0.29	0.66 ± 0.09	50	50	50
8	TSI-15-16	<i>p</i> -OCH <sub>3</sub>	<i>p</i> -OCH <sub>3</sub>	1- pyrazolyl	50	0.85 ± 0.95	50	50	50



**Table 3.**

In vivo pharmacokinetics (PK) of TSI-13-57. Mice were i.p. treated with TSI-13-57, and the serum concentrations of compound were determined during time to assess  $C_{max}$  (peak plasma concentration),  $T_{max}$  (time to reach  $C_{max}$ ),  $AUC_{all}$  (total area from zero to the last sampling time-point),  $V_d$  (Volume of distribution), Cl (Clearance) and  $t(1/2)$ (half-life).

	10 mg/kg (i.p.)	20 mg/kg (i.p.)
<b>Tmax (hours)</b>	0.25	4
<b>Cmax (nM)</b>	669	1260
<b>AUCall (hour*nmol)</b>	4781.9	19644.3
<b>Vd (mL)</b>	1190.3	N.A.
<b>Cl (mL/hour)</b>	84.2	42.5
<b>t(1/2) (hour)</b>	9.8	9

Author Manuscript

Author Manuscript

Author Manuscript

Author Manuscript

**Table 4.**

In vitro early ADMET analysis of TSI-13-57. CL<sub>int</sub>, intrinsic clearance. ADMET properties of TSI-13-57 were analyzed in vitro to assess suitability for in vivo applications.

Cytotoxicity EC <sub>50</sub> (μM)	<b>BJ</b>	<b>&gt;18.5</b>
	HEK293	>18.5
	HepG2	>18.5
	Raji	>18.5
Solubility (μM)	pH 7.4	14.4±5
Permeability (10e-6 cm/s)	pH 7.4	112.6±35
Stability mouse liver microsomes (t <sub>1/2</sub> (hours))		>4
CL <sub>int</sub> (ml/min/kg)		<13.5